

# **INVESTIGATION ON AN AIRBORNE MAGNETIC AND HELITEM SURVEY ON FLIN FLON AREA**

A Thesis Submitted to the College of  
Graduate and Postdoctoral Studies  
In Partial Fulfillment of the Requirements  
For the Degree of Master of Science  
In the Department of Geological Sciences  
University of Saskatchewan  
Saskatoon

By

Yu Han

©Copyright Yu Han, December, 2019. All rights reserved.

## **PERMISSION TO USE**

In presenting this dissertation in partial fulfillment of the requirements for a Postgraduate degree from the University of Saskatchewan, I agree that the Libraries of this University may make it freely available for inspection. I further agree that permission for copying of this thesis in any manner, in whole or in part, for scholarly purposes may be granted by the professor or professors who supervised my thesis work or, in their absence, by the Head of the Department or the Dean of the College in which my thesis work was done. It is understood that any copying or publication or use of this thesis or parts thereof for financial gain shall not be allowed without my written permission. It is also understood that due recognition shall be given to me and to the University of Saskatchewan in any scholarly use which may be made of any material in my thesis.

Requests for permission to copy or to make other uses of materials in this thesis in whole or part should be addressed to:

Head of the Department of Geological Sciences  
University of Saskatchewan  
114 Science Place  
Saskatoon, Saskatchewan S7N 5E2  
Canada

Dean  
College of Graduate and Postdoctoral Studies  
University of Saskatchewan  
116 Thorvaldson Building, 110 Science Place  
Saskatoon, Saskatchewan S7N 5C9  
Canada

## **ABSTRACT**

Over the past two decades, application of airborne time domain electromagnetic and magnetic technology has seen increased use in mineral and hydrocarbon exploration, ground water and environmental investigation, largely due to the characteristic that a moving platform is able to perform accurately and efficiently even in a varied and rough topography.

The helicopter-borne time domain electromagnetic system (HELITEM) is a new generation system designed and operated by Fugro Airborne Surveys. It has much larger peak current as well as peak dipole moment and later first gate compared with other airborne time domain electromagnetic (EM) technologies such as SkyTEM, VTEM and AeroTEM etc. Few studies has been published on HELITEM system. BFR Copper & Gold Inc. has made available a large HELITEM and magnetic survey of a volcanogenic massive sulfide (VMS) project in the Flin Flon area to be the data source of this study.

The induction of coil coupling over static geomagnetic field is firstly studied to determine if that would corrupt EM data, especially late gate signals. VMS targets are expected to be both conductive and magnetic. There are many examples of coincident magnetic and conductive anomalies in the data set. Therefore, coincident magnetic and conductive anomalies are searched to indicate target areas. Subsequently, forward and inversion plate models are created using modeling software Maxwell which was developed by ElectroMagnetic Imaging Technology (EMIT). Radial Spectrum method and tilt derivative method are applied for depth estimation using magnetic data and the results are compared with inversion models to find consistency and further determine whether the potential conductors should be investigated further.

The object of this research is to refine the search indirectly to determine which magnetic and conductive anomalies are coincident in depth as well as geographic location. Plate modeling on some of the more attractive targets is attempted to refine their depth, depth extent, size, shape and conductivity.

## **ACKNOWLEDGEMENTS**

Foremost, I would like to express my sincere gratitude to my supervisor Professor James Merriam for the continuous support of my master study and research, for his patience, motivation, enthusiasm, and immense knowledge. His guidance helped me in all the time of research and writing of this thesis. I could not have imagined having a better advisor and mentor for my master study.

Besides my supervisor, I would like to thank Professor Samuel Butler for his patience, encouragement, insightful comments and help to broaden my knowledge.

My sincere thanks also goes to Ms. Dawn Zhou and BFR Copper & Gold Inc, for providing the airborne magnetic and HELITEM survey data and funding for my master study.

Last but not the least, I would like to express my special thanks to my family for valuable encouragement and spiritual support during my studies.

## TABLE OF CONTENTS

<b>PERMISSION TO USE.....</b>	<b>I</b>
<b>ABSTRACT.....</b>	<b>II</b>
<b>ACKNOWLEDGEMENTS.....</b>	<b>III</b>
<b>LIST OF TABLES .....</b>	<b>VI</b>
<b>LIST OF FIGURES .....</b>	<b>VII</b>
<b>LIST OF EQUATIONS.....</b>	<b>X</b>
<b>1 INTRODUCTION AND BACKGROUND .....</b>	<b>1</b>
1.1 ELECTRICAL PROPERTIES OF ROCKS AND MINERALS.....	1
1.2 ELECTROMAGNETICS.....	4
1.3 AIRBORNETIME DOMAIN EM METHOD.....	4
1.4 VMS DEPOSIT.....	10
1.5 HELITEM SYSTEM .....	12
1.6 FLIN FLON AREA .....	15
1.7 MAXWELL SOFTWARE .....	17
<b>2 COIL COUPLING OVER STATIC EARTH FIELD.....</b>	<b>18</b>

2.1 INTRODUCTION.....	18
2.2 PROCEDURE.....	18
<b>3 CO-LOCATION OF EM AND MAG ANOMALIES.....</b>	<b>24</b>
3.1 INTRODUCTION.....	24
3.2 METHODS.....	26
3.2.1 Depth estimate from radial frequency spectrum method applied to magnetic data.....	26
3.2.2 Depth estimate from tilt derivative method applied to magnetic data.....	30
<b>4 MAXWELL PLATE MODELLING.....</b>	<b>34</b>
4.1 INTRODUCTION.....	34
4.2 PROCEDURE.....	36
<b>5 RESULTS.....</b>	<b>45</b>
<b>6 CONCLUSIONS.....</b>	<b>49</b>
6.1 RECOMMENDATIONS.....	50
<b>REFERENCES.....</b>	<b>51</b>

## LIST OF TABLES

<b>Table 1.1</b> Resistivity ( $\Omega\cdot\text{m}$ ) of some common semiconductor minerals.....	3
<b>Table 1.2</b> Range of time constant for earth materials with different electrical properties.....	9
<b>Table 1.3</b> Comparison of different airborne TEM systems.....	10
<b>Table 1.4</b> VMS ore minerals resistivity and magnetic susceptibility.....	11
<b>Table 1.5</b> Specification of HELITEM system.....	13
<b>Table 5.1</b> Comparison of depth estimate from electromagnetic anomalies and magnetic anomalies.....	48

## LIST OF FIGURES

<b>Figure 1.1</b> Range of electrical resistivity for different rock groups.....	3
<b>Figure 1.2</b> EM induction process of EM system.....	6
<b>Figure 1.3</b> Principle of time domain INPUT system. a) the primary magnetic field generated by the transmitter. b) receiver response to the primary field. c) decay of the secondary field is sampled at designated channels during off-time.....	8
<b>Figure 1.4</b> Coincident magnetic and conductive anomaly in Flight Line 12100.....	11
<b>Figure 1.5</b> Full view of HELITEM system.....	12
<b>Figure 1.6</b> Geometry of the HELITEM system.....	13
<b>Figure 1.7</b> Geology of the Flin Flon Greenstone Belt.....	16
<b>Figure 2.1</b> Calculated $dB/dt$ (nT/s) with respect to Easting (m) .....	19
<b>Figure 2.2</b> Calculated $dB/dt$ (nT/s) compared with observed $dB/dt$ (nT/s) with respect to Easting (m) .....	20
<b>Figure 2.3</b> Decay of Z component EM response (nT/s) with respect to time (ms) of a sample point as an example.....	21
<b>Figure 2.4</b> Fugro corrected the coil coupling effect as a part of leveling.....	21
<b>Figure 2.5</b> Calculated $dB/dt$ (blue) and $d^2B/dt^2$ (red) on Flight Line 12100.....	22
<b>Figure 2.6</b> Coil coupling effect varies at most about 3.4 nT/s during a pulse.....	23



<b>Figure 3.1</b> Co-location map of EM and MAG anomalies of Hollingdale Lake block.....	25
<b>Figure 3.2</b> Co-location map of EM and MAG anomalies of south Botham Bay block.....	25
<b>Figure 3.3</b> Hollingdale Lake sub-blocks division.....	27
<b>Figure 3.4</b> South Botham Bay sub-blocks division.....	28
<b>Figure 3.5</b> Examples of radial frequency spectrum laplace method.....	28
<b>Figure 3.6</b> Examples of radial frequency spectrum laplace method.....	29
<b>Figure 3.7</b> Depth estimation of Hollingdale Lake survey block.....	30
<b>Figure 3.8</b> Depth estimation of South Botham Bay survey block.....	31
<b>Figure 3.9</b> Tilt derivative contour map of a sub-block in south Botham Bay survey block.....	33
<b>Figure 4.1</b> Plate modelling with a 200m×200m thin plate and a depth of 75m. Flight direction is from left to right.....	35
<b>Figure 4.2</b> Location of Area 1.....	37
<b>Figure 4.3</b> Plate modelling of L30220 (Channels 15-30 are shown) .....	38
<b>Figure 4.4</b> Plate modelling of T30971 (Channels 15-30 are shown) .....	39
<b>Figure 4.5</b> Location of Area 2.....	40
<b>Figure 4.6</b> Plate modelling of L12080, L12090, L12100.....	42

<b>Figure 4.7</b> Profiles of the two-plate model comparing with field data (Channels 15-30 are shown) .....	43
<b>Figure 4.8</b> Plate modelling of T19080 (Channels 15-30 are shown) .....	44
<b>Figure 5.1</b> Radial frequency spectrum method applied to magnetic data in Area 1.....	46
<b>Figure 5.2</b> Radial frequency spectrum method applied to magnetic data in Area 2.....	46
<b>Figure 5.3</b> Tilt derivative method applied to magnetic data in Area 1.....	47
<b>Figure 5.4</b> Tilt derivative method applied to magnetic data in Area 2.....	47

## LIST OF EQUATIONS

Equation 1.1.....	2
Equation 1.2.....	2
Equation 1.3.....	4
Equation 1.4.....	4
Equation 1.5.....	4
Equation 1.6.....	4
Equation 1.7.....	4
Equation 1.8.....	7
Equation 1.9.....	7
Equation 1.10.....	7
Equation 1.11.....	7
Equation 1.12.....	7
Equation 2.1.....	19
Equation 3.1.....	26
Equation 3.2.....	26
Equation 3.3.....	26

<b>Equation 3.4</b> .....	26
<b>Equation 3.5</b> .....	30
<b>Equation 3.6</b> .....	31
<b>Equation 3.7</b> .....	31
<b>Equation 3.8</b> .....	32

# Chapter 1

## Introduction and Background

The object of this research is firstly studying the induction of coil coupling over static geomagnetic field to determine if that would corrupt EM data especially late gate signals. There are many examples of coincident magnetic and conductive anomalies in the data set. Therefore, coincident magnetic and conductive anomalies are searched to indicate target areas for volcanogenic massive sulfide deposits. Subsequently, forward and inversion plate models are created using modeling software Maxwell. Radial Spectrum method and tilt derivative method are applied for depth estimation using magnetic data and the results are compared with inversion models to find consistency and further determine whether the potential conductors should be investigated further. Plate modeling on some of the more attractive targets is attempted to refine their depth, depth extent, size, shape and conductivity.

### 1.1 ELECTRICAL PROPERTIES OF ROCKS AND MINERALS

The electrical properties of rocks and minerals underground are the most basic and frequently used characteristic for geophysical exploration. Resistivity and conductivity are most likely to be referred to in those cases. According to Ohm's Law, a uniform conductor's resistance is inversely proportional to the cross-sectional area and proportional to its length:

$$R = \rho \frac{L}{A} \quad 1.1$$

where  $R$  is resistance in  $\Omega$ ,  $L$  is the length of the conductor in m,  $A$  is the cross-sectional area of the conductor measured in  $m^2$ , and  $\rho$  is the electrical resistivity of the material in  $\Omega \cdot m$ .

Resistivity and conductivity are reciprocals:

$$\rho = \frac{1}{\sigma} \quad 1.2$$

where  $\sigma$  is the electrical conductivity measured in S/m.

Rocks and ores are composed of minerals whose resistivity can range over many orders of magnitude. Native metals usually have extremely low resistivity: native gold (Au) has a resistivity of about  $2 \times 10^{-8} \Omega \cdot m$ ; native copper (Cu) has a resistivity of about  $1.2 \times 10^{-8} \sim 30 \times 10^{-8} \Omega \cdot m$  and graphite's resistivity is as low as  $10^{-6} \Omega \cdot m$  (Robert, 1989). Compared to native metals, semiconductor minerals have a higher range of resistivity, as shown in Table 1.1. According to the table, chalcopyrite, pyrite and galena have low resistivity (lower than  $1 \Omega \cdot m$ ) which means they are good conductors.

When it comes to different types of rocks and ore bodies, their electrical resistivity shows a greater range of as much as 7 orders of magnitude. Figure 1.1 shows some typical ranges of different rock groups' resistivity (Palacky, 1987). Igneous and metamorphic rocks, of which the Canadian Shield (also called the Laurentian Plateau) is mainly composed, show a high resistivity of  $10^3 \sim 10^5 \Omega \cdot m$ ; sedimentary rocks have a relative low resistivity while massive sulfides are most conductive with resistivity below  $1 \Omega \cdot m$ . Therefore, volcanogenic massive sulfide (VMS) deposits are expected to be conductive with respect to any host.

Mineral	Resistivity ( $\Omega \cdot m$ )	Mineral	Resistivity ( $\Omega \cdot m$ )
Bornite	1.6 to $6000 \times 10^{-6}$	Hematite	$10^2$
Magnetite	$52 \times 10^{-6}$	Cassiterite	$4.5 \times 10^{-4}$ to 10000
Pyrrhotite	2 to $160 \times 10^{-6}$	Stibnite	$10^6$
Chalcopyrite	150 to $9000 \times 10^{-6}$	Pyrolusite	0.007 to 30
Pyrite	1.2 to $600 \times 10^{-3}$	Siderite	$8.3 \times 10^9$
Galena	$6.8 \times 10^{-6}$ to $9 \times 10^{-2}$	Chromite	$5 \times 10^7$
Chalcocite	80 to $100 \times 10^{-6}$	Sphalerite	$2.7 \times 10^{-3}$ to $1.2 \times 10^4$
Molybdenite	0.12 to 7.5	Ilmenite	0.001 to 4

Table 1.1 Resistivity ( $\Omega \cdot m$ ) of some common semiconductor minerals. Resistivity of Hematite, Stibnite, Siderite and Chromite are after Touloukian (1989), and the resistivity of other minerals are after Robert (1989).

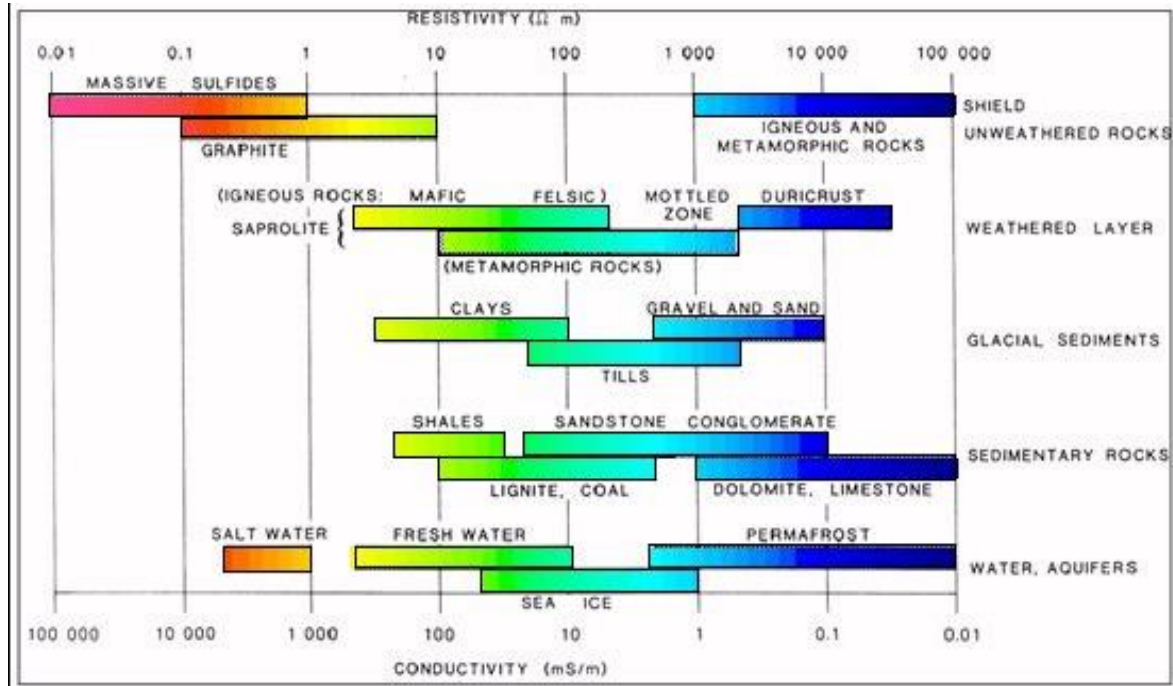


Figure 1.1 Range of electrical resistivity for different rock groups. After Palacky (1987)

## 1.2 ELECTROMAGNETICS

This part is about the basic theory of the airborne electromagnetism system that has been approached in this study. The foundation of classic electromagnetism is unified by James Clerk Maxwell who published an early form of a set of partial differential equations between 1861 and 1862. The Maxwell equations are used to describe how electric and magnetic fields behave in media (Edward, 2018):

$$\nabla \times \mathbf{E} = -\frac{\partial \mathbf{B}}{\partial t} \quad 1.3$$

$$\nabla \times \mathbf{H} = (\mathbf{J} + \varepsilon \frac{\partial \mathbf{E}}{\partial t}) \quad 1.4$$

$$\nabla \cdot \mathbf{B} = 0 \quad 1.5$$

$$\nabla \cdot \mathbf{D} = \rho_c \quad 1.6$$

where  $\mathbf{E}$  is the electric field intensity in V/m,  $\mathbf{B}$  is the magnetic field density in the unit of T,  $\mathbf{H}$  is the magnetic flux intensity in A/m,  $\mathbf{J}$  is the current density in A/m<sup>2</sup>,  $\varepsilon$  is the dielectric permittivity in F/m,  $\mathbf{D}$  is the dielectric displacement in the unit of C/m<sup>2</sup> and  $\rho_c$  is the electric charge density in C/m<sup>3</sup>. The vectors' relations with each other are :

$$\mathbf{B} = \mu \mathbf{H}, \mathbf{D} = \varepsilon \mathbf{E}, \mathbf{J} = \sigma \mathbf{E} \quad 1.7$$

where  $\mu$  is the magnetic permeability in H/m and  $\sigma$  is the conductivity in the unit of S/m. When the medium is free space, the magnetic permeability equals  $4\pi \times 10^{-7}$  H/m and the dielectric permittivity will be approximately  $8.85 \times 10^{-12}$  F/m.

## 1.3 AIRBORNE TIME DOMAIN EM METHOD



Canadian mining exploration companies started to develop airborne electromagnetic (EM) systems in the early 1950s for the purpose of searching for conductive ore bodies in an efficient manner even in a varied and rough topography (Richard, 2010). It has been proven successful in locating massive sulphide deposits hosted in resistive terrain such as the Canadian Shield (Keating, 1988). Gradually this method was applied in other areas such as finding groundwater, hydrocarbons and other mineral deposits with the improvement of digital acquisition systems, noise reduction processes and data interpretation methods (Richard, 2010). Historically many types of configurations have been applied in airborne electromagnetic methods. Two general groups of the techniques are time domain EM methods and frequency domain EM methods. For the first type, time is an explicit independent variable in contrast to frequency domain EM. And we focus on time domain EM in this work.

Electromagnetic induction is the theory foundation of airborne EM systems. Two essential parts of any EM system would be a transmitter and a receiver (Figure 1.2). After an alternating current is injected in the transmitter, a vortex of time-varying magnetic fields will be generated. This is called the primary field. If there is a conductor underground, the vortex of magnetic fields will induce another time-varying (eddy current) current inside the conductor. And again according to Faraday's Law, this eddy current will create a new set of magnetic fields called the secondary field. The receiver detects the signal of the secondary field and it will be important to assist in locating and estimating the conductor. It is noteworthy that the primary field which travels through air and ground will also be detected by the receiver (Reynolds, 1997). Therefore separating the primary and secondary fields is important before interpretation of the signal since only the secondary field contains information on the conductive target. One good approach to avoid the disturbance from the primary field is to measure the signal when the transmitter current is off (off-time). This is also the main advantage of time domain EM over frequency domain EM. Figure 1.3 illustrates an example of one such system. After the transmitter current is turned off, the decay of the secondary field (usually the time derivative of it) is measured at several designated time intervals (channels). How fast the secondary field decays indicates how conductive the potential target is (Jean 2015).

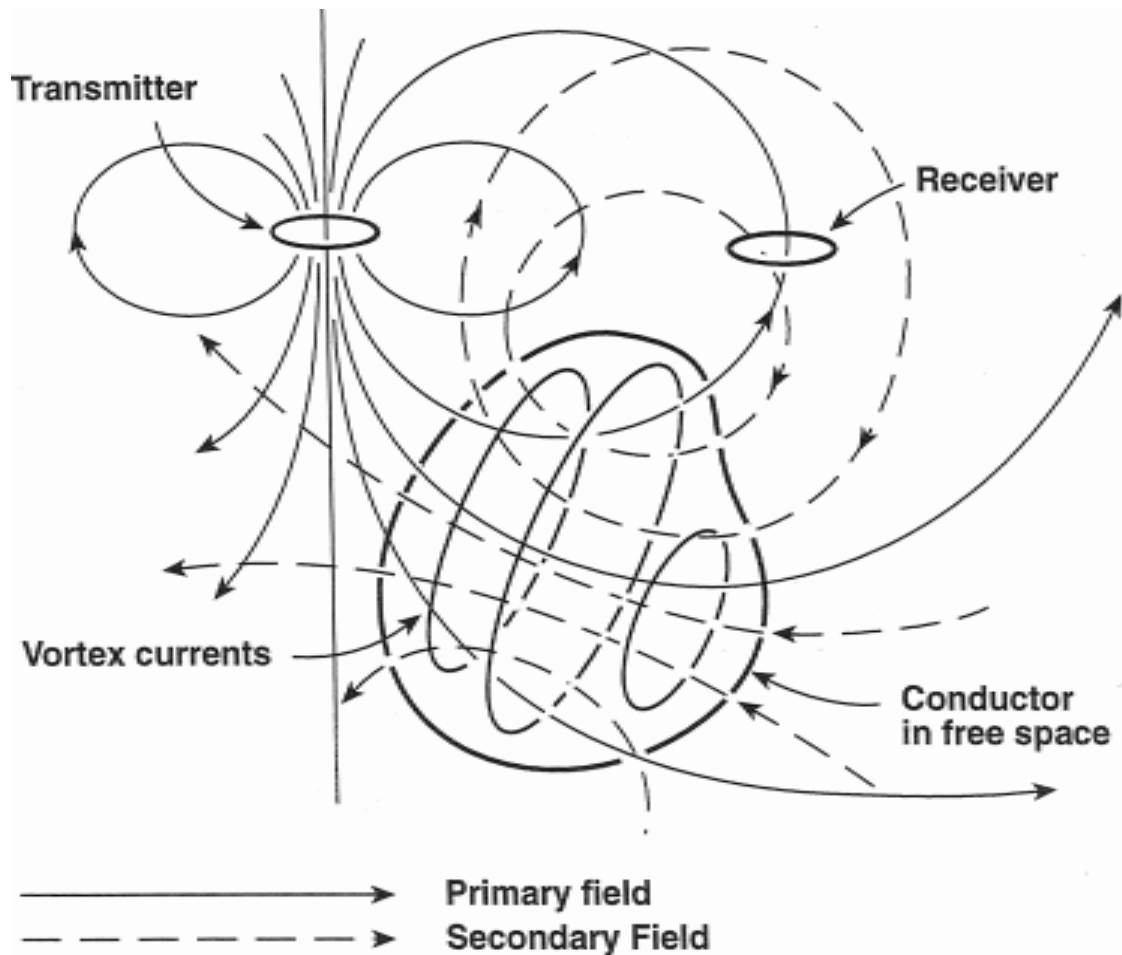


Figure 1.2 EM induction process of EM system. After Grant and West (1965)

The decay of the off-time secondary signal is complex but can be conveniently delineated into early time, intermediate time and late time. In early time the current is flowing only on the outside of the target and is beginning to diffuse into the target. In intermediate time the current is diffusing well into the target and decaying at a diffusion controlled rate, that is as a power law of  $t^{-1/2}$ . In late time the current density is nearly uniform throughout the target and the signal decays exponentially in time. Late time data is the most informative because the time constant depends on the resistivity and dimensions of the target.

$$V = V_0 \cdot e^{-\frac{t}{\tau}} \quad 1.8$$

where  $V$  is the receiver signal from the secondary field,  $V_0$  is the initial value,  $t$  is time in microseconds and  $\tau$  (tau) is the decay constant (or time constant) in microseconds. A semi-log plot of this function will be displayed as a straight line and its slope can be obtained. If two points on the line is taken, equation 1.8 will become:

$$V_1 = V_0 \cdot e^{-\frac{t_1}{\tau}} \quad 1.9$$

$$V_2 = V_0 \cdot e^{-\frac{t_2}{\tau}} \quad 1.10$$

Taking the base  $e$  log of the ratio of the above two equations:

$$\ln \frac{V_1}{V_2} = \frac{t_2 - t_1}{\tau} \quad 1.11$$

$$\begin{aligned} \tau &= \frac{t_2 - t_1}{\log_{10} e \times \log_{10} \frac{V_1}{V_2}} \\ &= -\frac{1}{\log_{10} e \times slope} \end{aligned} \quad 1.12$$

where *slope* is the slope of the semi-log plot of the receiver signal.

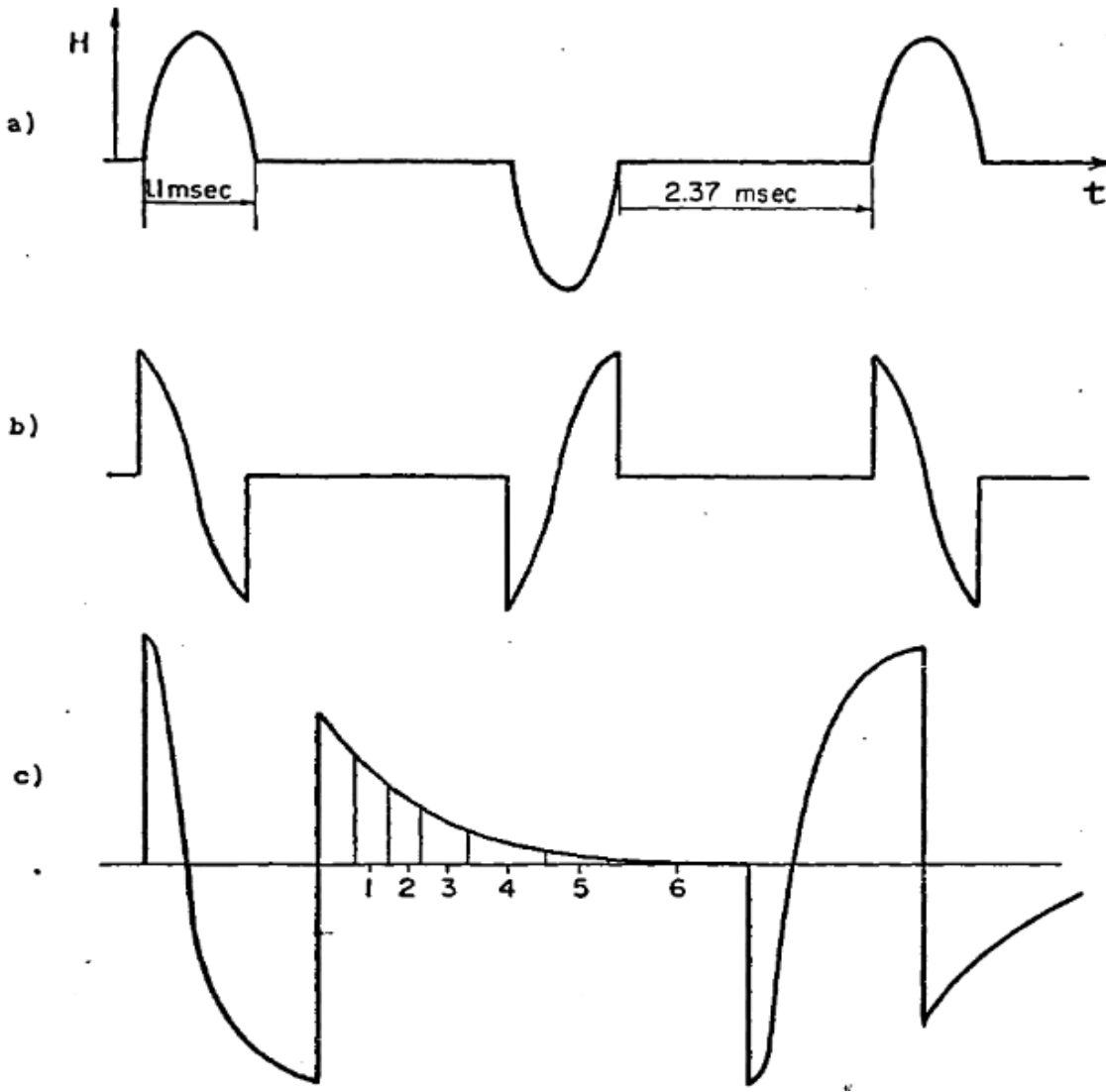


Figure 1.3 Principle of time domain INPUT system. a) the primary magnetic field generated by the transmitter. b) receiver response to the primary field. c) decay of the secondary field is sampled at designated channels during off-time (Ghosh, 1972)

Different types of conductors and semiconductors have different ranges of time constants which makes time constant a very useful parameter to indicate the peak position of response and also how conductive the target is. Jinming (2005) summarized how time constant and electrical properties relate based on field surveys (Table 1.2).

$T/\mu\text{s}$	Type	Materials
<100	weak conductor	igneous rock, metamorphic rock, sphalerite, fresh water etc.
100~200	moderate conductor	Salt water, clay, shale, serpentinite etc.
200~1000	good conductor	magnetite, graphite, some sulfide minerals etc.
>1000	best conductor	sulfide ore, metallic minerals:copper, gold, silver etc.

Table 1.2 Range of time constant for earth materials with different electrical properties

Therefore the better the conductor is, the larger value of decay constant it will have, which means the slower the secondary field will decrease in late time.

There are many configurations currently in use for airborne time domain EM systems after a long history of development and update. Helicopter-borne systems are used more and more widely as a helicopter platform can fly at lower height and therefore investigate in greater detail. Usually helicopter-borne systems use a “tow-bird” configuration (Reynolds, 1997), which tows a large transmitter loop beneath the aircraft and has a receiver dipole placed above, inside or behind the transmitter loop. Table 1.3 lists the specifications and parameters of some common helicopter-borne time domain EM systems (“Airborne TEM systems”, 2017). In this work, data from HELITEM system was obtained and studied.

The higher the dipole moment is, the deeper the system can investigate and the decay can be traced far larger. Therefore different configurations can serve different exploration purpose from near surface to several hundreds of meters underground.

Parameter/System	SkyTEM	AeroTEM	VTEM	HELITEM
Number of turns in transmitter loop	1-16	8	4	2
Pulse shape	square wave, dual transmitter mode	triangular	polygonal	half-sine
Peak current, A	120	250	310	1412
Peak dipole moment, $\times 1000$ NIA	3, 4, 32, 150, 500, 1000	40, 340, 1000	240, 625, 1300	2000
First gate, $\mu$ s	4		13	175

Table 1.3 Comparison of different airborne TEM systems

## 1.4 VMS DEPOSIT

In this study, the potential targets are volcanogenic massive sulfide (VMS) deposits. VMS deposits are formed submarine after volcanic and hydro-thermal processes (Yusheng et al., 2011) and their major composing minerals include chalcopyrite, pyrite, magnetite and galena. VMS deposits have a high economic value because they are the major sources of zinc, copper, lead and they could also have byproducts such as gold and silver. As shown in Table 1.4, those associated minerals tend to have a quite low range of resistivity and magnetite is so magnetic explaining why VMS deposits are very likely to be conductive as well as magnetic. The huge difference between electrical properties of VMS deposit and its hosting environment becomes a great advantage that can be used in geophysical exploration. There are many examples of potential coincident magnetic and conductive anomalies in the data set (Figure 1.4 shows a potential coincident magnetic and conductive anomaly in same geographic location and whether they are in same depth or not will be looked at later in the study).

Mineral	Resistivity <sup>1</sup> ( $\Omega \cdot m$ )	Susceptibility <sup>2</sup> ( $*10^{-3}$ SI)
Chalcopyrite	150 to $9000 \times 10^{-6}$	0.4
Pyrite	$1.2$ to $600 \times 10^{-3}$	5
Pyrrhotite	$2$ to $160 \times 10^{-6}$	3200
Sphalerite	$2.7 \times 10^{-3}$ to $1.2 \times 10^4$	0.8
Galena	$6.8 \times 10^{-6}$ to $9 \times 10^{-2}$	-0.03
Magnetite	$52 \times 10^{-6}$	5700
Hematite	$10^{-3} \sim 10^6$	40

Table 1.4 VMS ore minerals resistivity and magnetic susceptibility. <sup>1</sup>Resistivities from Robert (1989).

<sup>2</sup>Susceptibilities from Hunt et al. (1995).

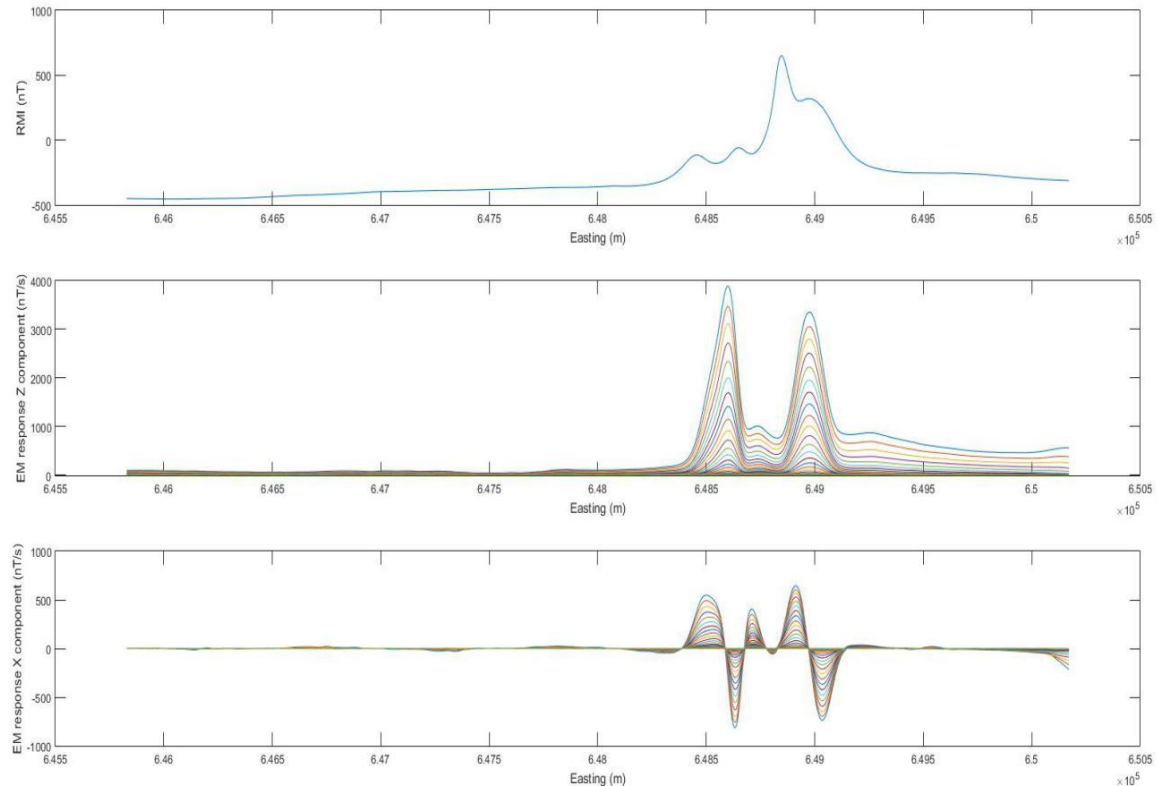


Figure 1.4 Coincident magnetic and conductive anomaly in Flight Line 12100. The top subplot is residual magnetic intensity (nT); the middle subplot is z component EM response (nT/s); the bottom subplot is x component EM response (nT/s).

## 1.5 HELITEM SYSTEM

HELITEM system is a relative new system developed by Fugro Airborne Surveys (merged by CGG in 2013). Few studies have been published on this system to date, but it is becoming widely used. Figure 1.5 and 1.6 present a working HELITEM system and Table 1.5 lists specification of the system (Fugro Airborne Surveys, 2013).



Figure 1.5 Full view of HELITEM system



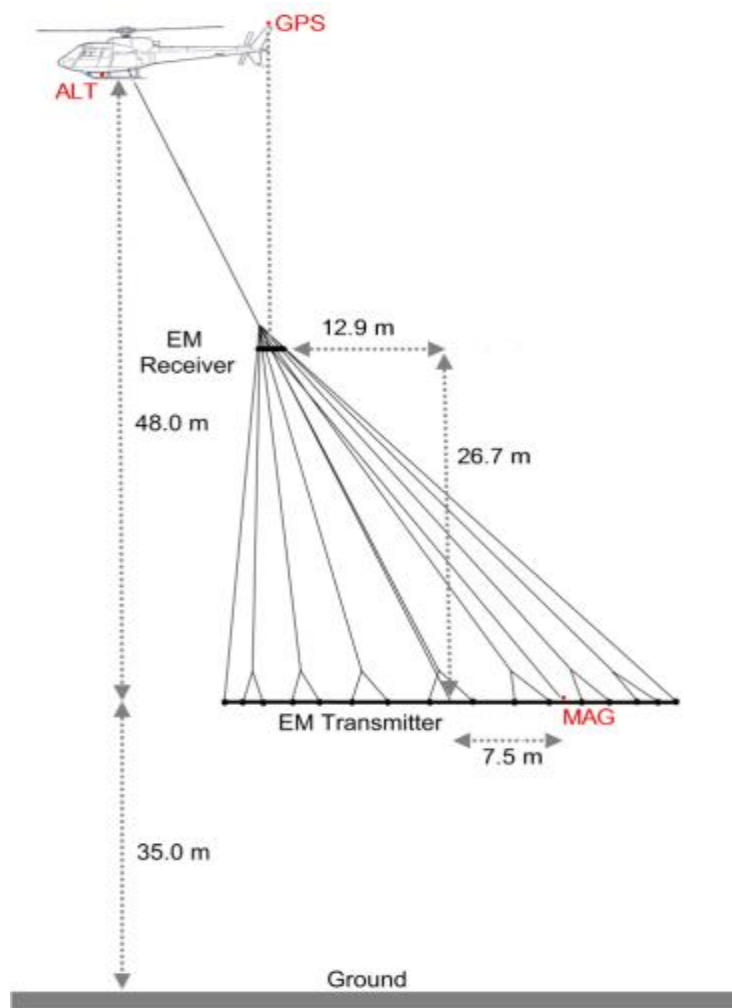


Figure 1.6 Geometry of the HELITEM system

Parameter	HELITEM
Transmitter area per turn / $\text{m}^2$	708
Number of turns	2
Pulse shape	half-sine
Peak current / A	1412
Peak dipole moment / $\text{A}\cdot\text{m}^2$	$2\times 10^6$
Frequency / Hz	30
Measured field components	Z, X, Y
Flying speed / (km/h)	90

Table 1.5 Specification of HELITEM system.

The survey area was divided by flight lines that are East-West directions and tie lines that are North-South directions. Two adjacent flight lines are 100 meters apart and two adjacent tie lines are 1000 meters apart. The helicopter flew along the flight lines and tie lines to collect all the data.

Airborne time domain electromagnetic surveys tend to apply high dipole moment and this HELITEM system used a peak dipole moment as high as  $2 \times 10^6 \text{ A} \cdot \text{m}^2$  (Table 1.5). One reason for this is that it will be hard to do many stacks on one sampling point while the aircraft is flying (stacking is summing repeat measurements over time to reduce random noise). Compared to airborne TEM method, the ground methods can do many stacks at each sampling point so they can use a smaller dipole moment.

According to the the logistics report from Fugro Airborne Surveys (2013), a two-turn transmitter loop which is towed 48m below the helicopter carries a set of discontinuous sinusoidal pulses and generates the primary field. The advantage of sinusoidal pulses over square pulse waves is that sinusoidal pulses can make the on-time response measurable as well as the off-time response. The base frequency is selectable and in this survey the frequency is set to be 30 Hz. After each current pulse is injected and primary field created, a secondary field is generated from the eddy current in the ground and the receiver will sense the electromagnetic response caused by the secondary field. By definition the primary is what the receiver senses in the absence of any conductors and the secondary is what the receiver senses from the currents in the conductors. The receiver sensor is suspended 26.7m above and 12.9 ahead of the transmitter loop while flying and it can measure three components (Z, X, Y) of the secondary response. There are 4 on-time channels and another 26 channels to record the off-time signal. The HELITEM system also brings a high sensitive magnetometer which means a magnetic survey can be conducted at the same time. Minerals like magnetite and pyrrhotite could be contained in sulfide ore bodies and their magnetic properties determine that a magnetometer is able to assist in detecting them.

Several factors together raise the practicability, depth of penetration and signal-noise ratio of HELITEM system: its transmitter loop carries pulses with a 1412 A peak current and peak dipole

moment is as high as  $2 \times 10^6 \text{ A} \cdot \text{m}^2$  (Table 1.5) which is the largest among all airborne systems in the industry; The platform flies at a quite low height and hence a shorter distance between the transmitter / receiver and the ground is settled; the concentration of measurement is on the decaying secondary response when the primary field is off (off-time).

It also should be noted that several procedures are performed in the field as data are collected (Fugro Airborne Surveys, 2013).

- 1) Digital Stacking. Broadband noise can be suppressed through stacking. It should be noticed that the system has limit number of stacks because the aircraft moves fast.
- 2) Windowing of data. This process is to arrange the time gates (in this survey 30 gates) for sampling properly.
- 3) Primary field. The spatial relation between the transmitter and the receiver might be changed throughout the flight. Thus the receiver records the primary field for each stack to assess the noise from geometry fluctuation (varying separation and alignment of coils).

## **1.6 FLIN FLON AREA**

Flin Flon is a Mining city lying on the border of Saskatchewan and Manitoba. It has a 90 year history of exploration and mining activities and is still attracting mining companies to come back with improved detecting techniques. Hudson Bay Mining & Smelting Co. Limited started mining and exploration in Flin Flon area in 1927 for copper and zinc ore resources and achieved great success which led the subsequent history of exploration work (“Flin Flon History”, 2017).

This section introduces briefly the regional geology of Flin Flon area. The survey blocks are located in the Hanson Lake Assemblage of the west part of Flin Flon Greenstone Belt (Dawn, 2013; Galley et al., 2007), as shown in Figure 1.7.

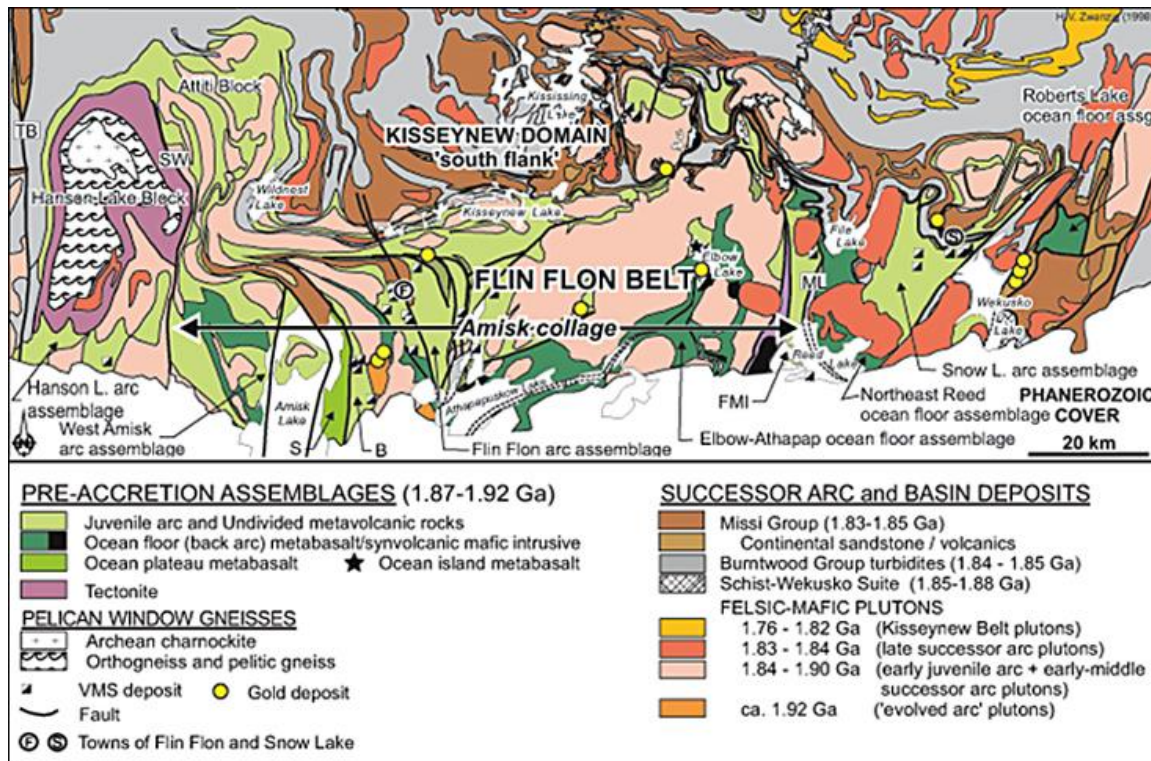


Figure 1.7 Geology of the Flin Flon Greenstone Belt. After Galley et al. (2007)

Flin Flon Greenstone Belt (also called Flin Flon-Snow Lake Greenstone Belt) was formed in the Paleoproterozoic period by arc volcanism and is part of the Trans-Hudson Orogen which is a suture zone leading to the formation of the Canadian Shield (Simard et al., 2013). According to recent study, a quite intact tectonostratigraphic record is preserved within the Trans-Hudson Orogen from early ca. 2.45-1.95 Ga rift to formation of juvenile crust at about ca. 2.0-1.88 Ga, and to the collisional basins and the following volcano arcs at about 1.88-1.83 Ga (Gibson et al 2013). The Flin Flon Belt is composed of a series of assemblages including juvenile arc, ocean-floor back arc, ocean plateau, oceanic island basalt etc. The volcanic rocks of the arc assemblage are mainly mafic. However, great quantity of volcanogenic massive sulfide ores are found associated with the arc assemblage's felsic volcanic units, which as a result made the Flin Flon Greenstone Belt one of the largest VMS mining district in the world. Many VMS and gold deposits have been detected and mined in this area.

## **1.7 MAXWELL SOFTWARE**

Maxwell is a 32-bit windows software for the modeling of geophysical electromagnetic data developed by ElectroMagnetic Imaging Technology (EMIT). It is widely used in the industry and it is the application that this study used for thin plate modeling. Maxwell can deal with many types of geophysical electromagnetic data, including time-domain EM and frequency-domain EM, data acquired in a ground survey, in a flying platform or down a drillhole (“Maxwell - Industry Standard Geophysical EM Data Modeling - EMIT”, 2017). Maxwell allows users to select among 6 model types: layered earth, multiple plates, integral equation prisms, 2.5D finite element, 3D finite element and wire filaments (some of them need additional external package). It is convenient to perform both forward and inverse modeling with Maxwell and it has a relatively fast computation speed which is a great advantage for people who have large data sets.

# Chapter 2

## Coil Coupling Over Static Earth Field

### 2.1 INTRODUCTION

According to the Faraday's Law, when the magnetic flux through a closed loop changes, an electromotive force is induced in the loop proportional to the rate of change of the flux. The HELITEM data were generated through a helicopter-borne time-domain EM system. As the transmitter and receiver coils are attached to a flying helicopter instead of being fixed at one spot, there will be an induced  $\frac{dB}{dt}$  ( $B$  is the magnetic field,  $t$  is time) produced as a result of the motion of the coils in the geomagnetic field and this induced  $\frac{dB}{dt}$  is called the coil coupling effect in this study. Fugro Airborne Surveys corrected this electromagnetic induction as a part of the leveling. We want to make sure if this correction is sufficient and if not, to what extent will this corrupt the late time data.

### 2.2 PROCEDURE

In order to know if the induced  $\frac{dB}{dt}$  is eliminated correctly, first I calculated the induced  $\frac{dB}{dt}$  from the latitude-corrected magnetic field data and compare it with the EM response obtained by the receiver. I took the flight line L12100 in south Botham Bay block as an example calculation.

According to

$$\frac{dB}{dt} = \frac{dB}{dx} \cdot \frac{dx}{dt} \quad 2.1$$

where  $x$  is the position of the receiver,  $B$  is the magnetic field,  $\frac{dx}{dt}$  is the velocity of the helicopter and  $\frac{dB}{dx}$  is the derivative of the magnetic field with respect to the position of the receiver. Then  $\frac{dB}{dt}$  can be calculated. (Figure 2.1)

We can see that the calculated  $\frac{dB}{dt}$  changes very quickly at some sampling points. We can also observe a difference between the calculated  $\frac{dB}{dt}$  and the  $\frac{dB}{dt}$  z component generated by the receiver from different channels as shown in Figure 2.2.

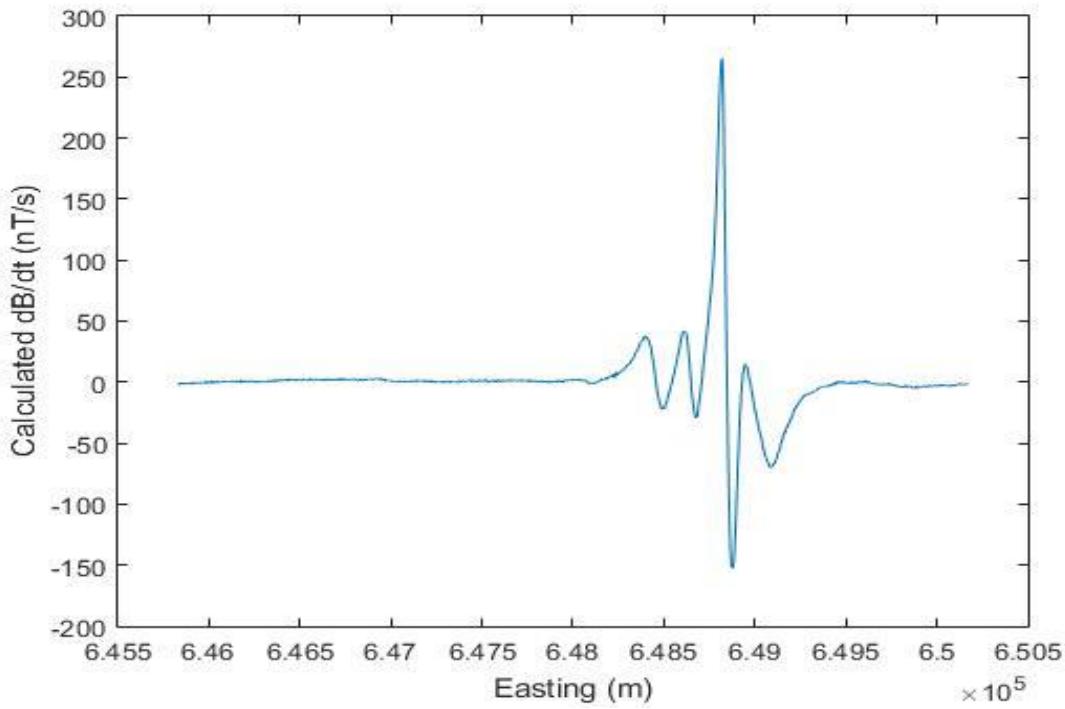


Figure 2.1 Calculated dB/dt (nT/s) with respect to Easting (m)

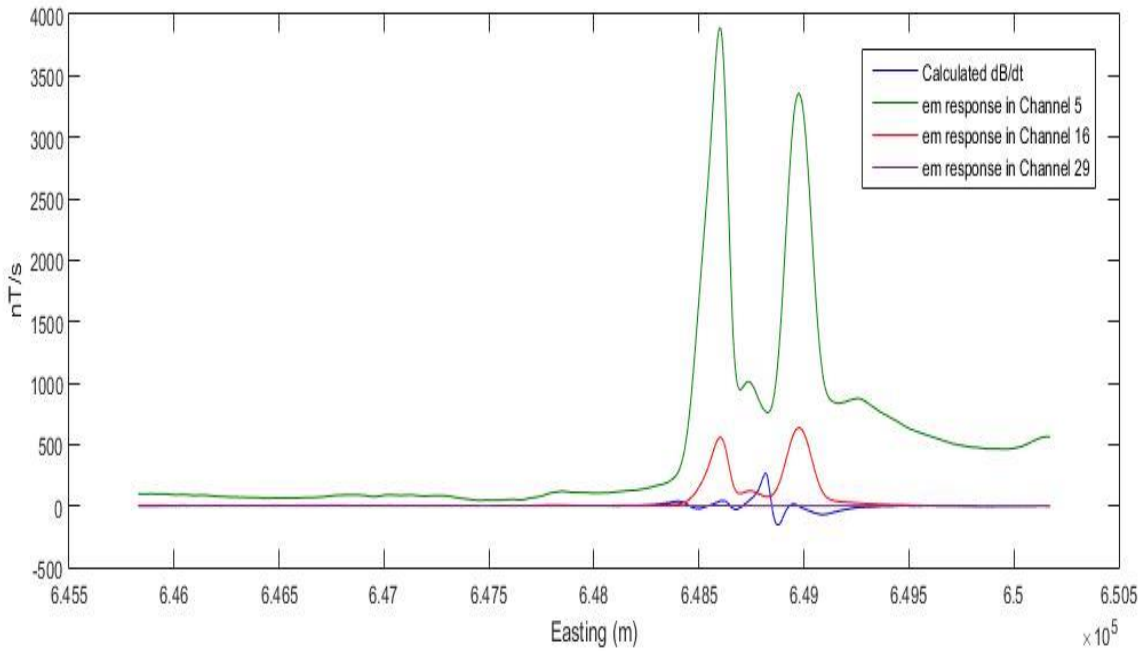


Figure 2.2 Calculated dB/dt (nT/s) compared with observed dB/dt (nT/s) with respect to Easting (m)

The blue line is the calculated  $\frac{dB}{dt}$ . And the green, red, purple lines separately represent  $\frac{dB}{dt}$  z component generated by the receiver from the first off-time channel (channel 5), a middle channel (channel 16) and a late channel (channel 29). There is a obvious decay from channel 5 to channel 29. Compared to the Z component EM response, the coil coupling effect is very much smaller than the first channel secondary response, comparable to the middle channel secondary response and larger than the late channel secondary response.

If we take a sample point as an example, the decay of the Z component EM response is shown below in Figure 2.3. As we can see, the late gates data didn't decay to zero as they should. They are raised by a certain amount because of the coil coupling effect. Fugro corrected this effect as a part of leveling, which means they assumed that the coil coupling effect is a constant during a pulse time and then subtracted the constant from all channels of data to bring the last channel of data to zero (as shown in Figure 2.4).



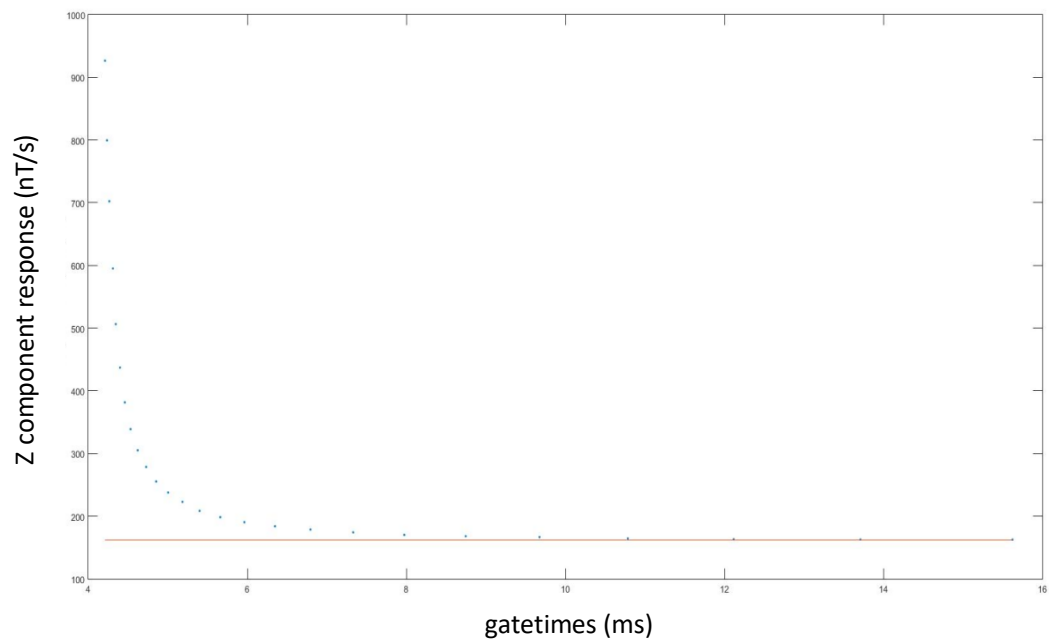


Figure 2.3 decay of Z component EM response (nT/s) with respect to time (ms) of a sample point as an example

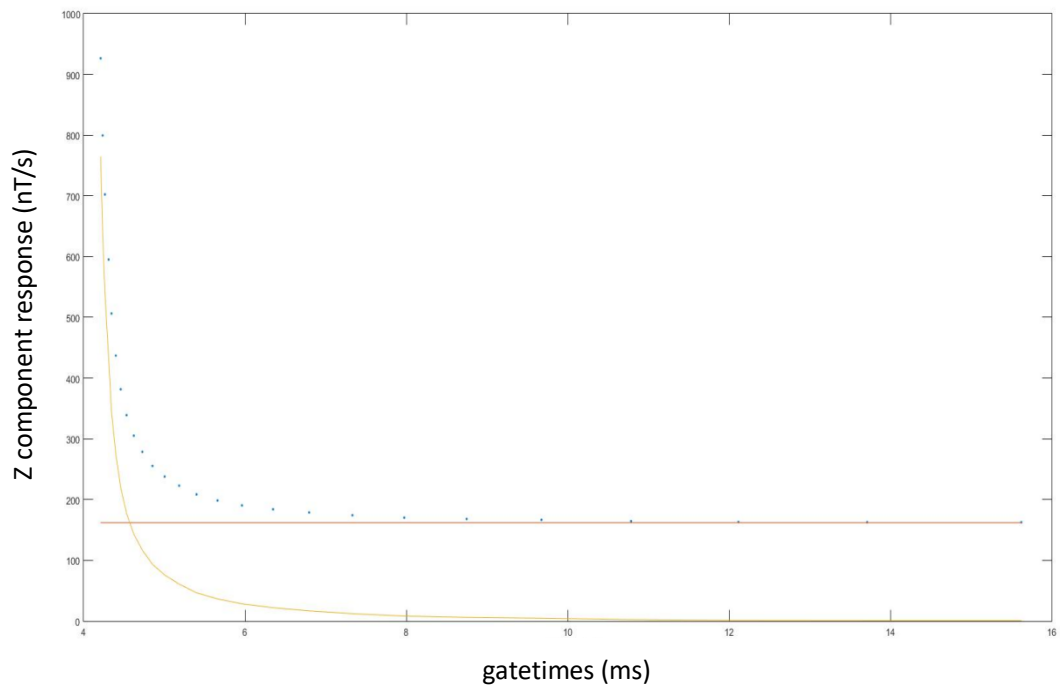


Figure 2.4 Fugro corrected the coil coupling effect as a part of leveling

The question is: Is the coil coupling effect a constant during a pulse?

$\frac{d^2B}{dt^2}$  is the linear rate of change of calculated  $\frac{dB}{dt}$  and is obtained from calculated  $\frac{dB}{dt}$  (as shown in Figure 2.5). The largest value of  $\frac{d^2B}{dt^2}$  is 264.25 nT/s<sup>2</sup> and if we multiplied it by the length of a pulse (13ms), we can get the largest linear change rate of this coil coupling effect over a pulse which is 3.435 nT/s in this case.

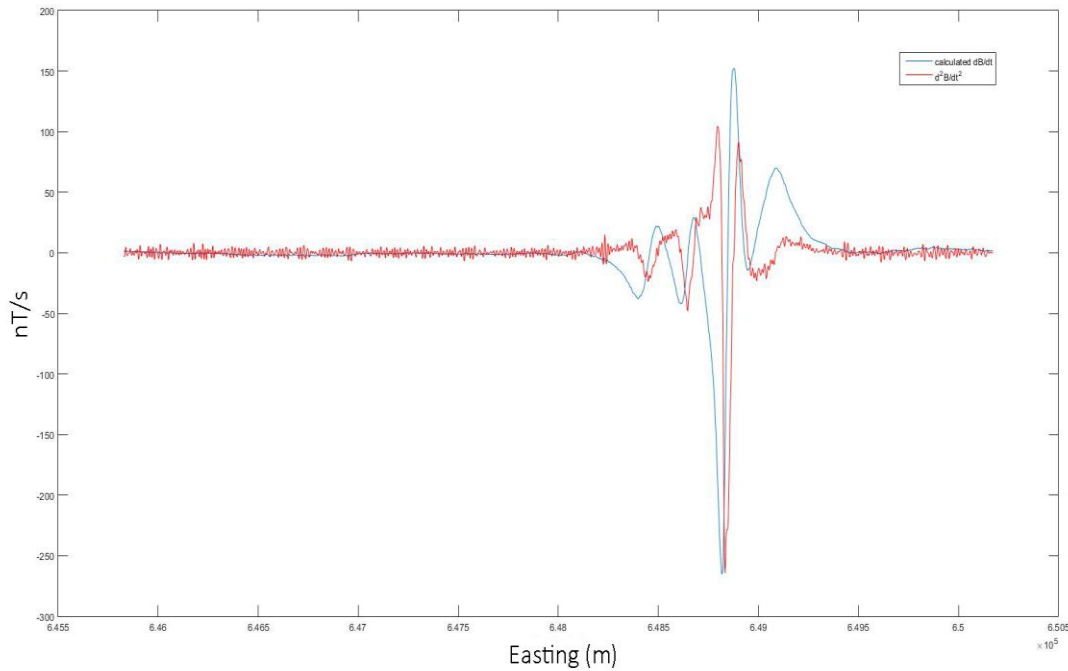


Figure 2.5 Calculated dB/dt (blue) and d<sup>2</sup>B/dt<sup>2</sup> (red) on Flight Line 12100

Therefore instead of being a constant, coil coupling effect changes at most about 3.4 nT/s during a pulse (Figure 2.6) and this value is considerable compared to the late gates of EM response. In this example, large horizontal gradient in B field and small time constant for the secondary response can result in serious coil coupling issue. Simply subtracting a constant to correct the coil coupling effect is not sufficient.

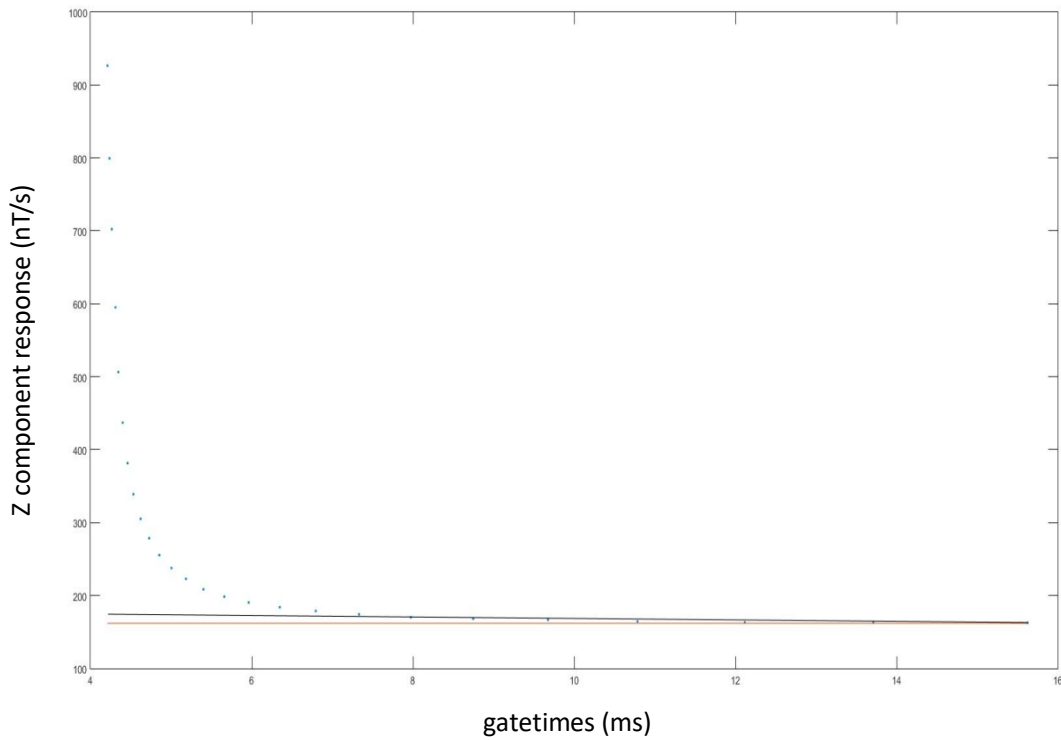


Figure 2.6 Coil coupling effect varies at most about 3.4 nT/s during a pulse

However, we cannot perform a better correction of the coil coupling effect because the HELITEM system doesn't measure the vertical component of the magnetic field and as a result we don't have the Z component magnetic field data to use for calculation in Equation 2.1 in order to compare with Z component EM response. The HELITEM system only measures the total magnetic field and I used it in the above calculation. If the Z component magnetic field data is obtained and used, the coil coupling effect would be a smaller value, but we did prove that the coil coupling effect cannot be viewed as a constant during a pulse time. The first several channels may not be effected a lot because the amplitude of their responses is usually high compared to the induced  $\frac{dB}{dt}$ , but to the late channels the coil coupling effect could be big enough to be concerned about. And as a consequence of this misinterpretation, some time constants might be poorly constrained, especially in the case of deposits with long time constants and high horizontal magnetic gradients.

# Chapter 3

## Co-location of EM and Mag Anomalies

### 3.1 INTRODUCTION

Volcanogenic massive sulfide (VMS) deposits are the potential targets in this study. According to Table 1.4, it is known that VMS deposits are very likely to be conductive as well as magnetic compared to their hosting environment. Therefore in the electromagnetic and magnetic survey, we are looking for anomalous signals that are conductive and magnetic coincidentally.

Co-location maps of electromagnetic and magnetic anomalies of Hollingdale Lake block and south Botham Bay block were generated separately (Figure 3.1 and Figure 3.2). Contour maps of residual magnetic intensity (RMI) are used as base maps for Figure 3.1 and Figure 3.2 and the red circles indicate where electromagnetic anomalies and magnetic anomalies exist at the same location.

Electromagnetic (EM) anomalies may be caused by near surface layers while magnetic anomalies may be reflecting the deeper bedrock structures. The figures below only showed that the magnetic and electromagnetic anomalies are in the same location, not necessarily at the same depth. The signals that are wanted are where the magnetic anomaly and electromagnetic anomaly are responding to the same source, which means they are not only from the same location, but also the same depth. This chapter discussed firstly the location of the coincidental electromagnetic and magnetic anomalies and secondly depth estimate from the magnetic data.

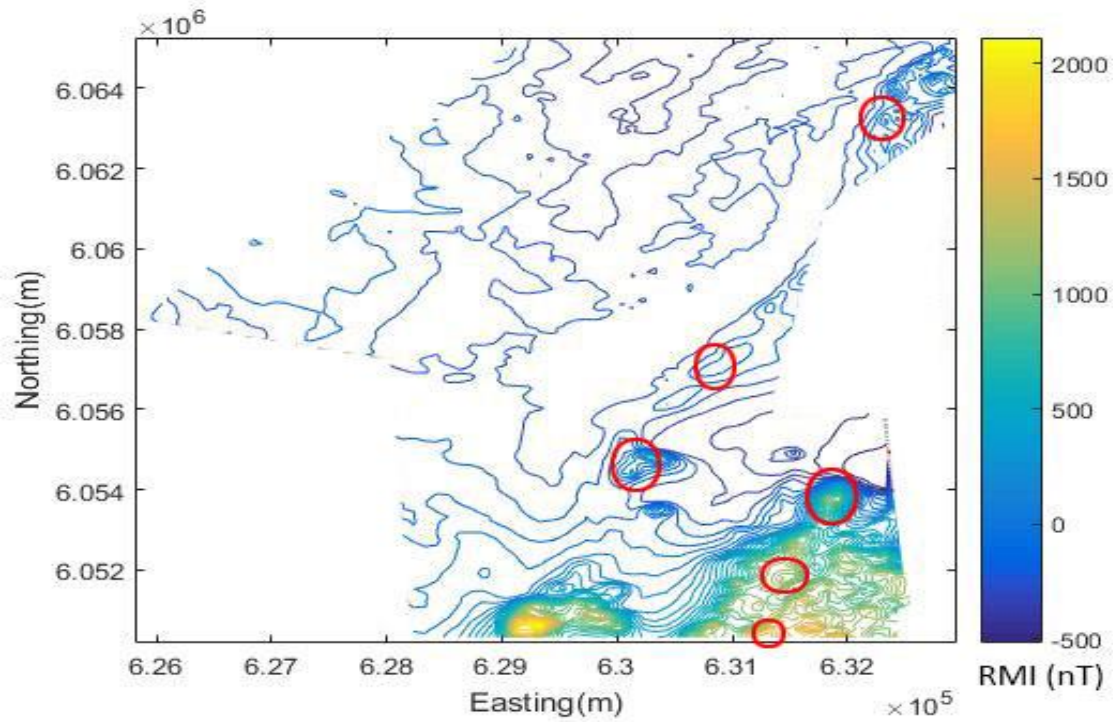


Figure 3.1 Co-location map of EM and MAG anomalies of Hollingdale Lake block

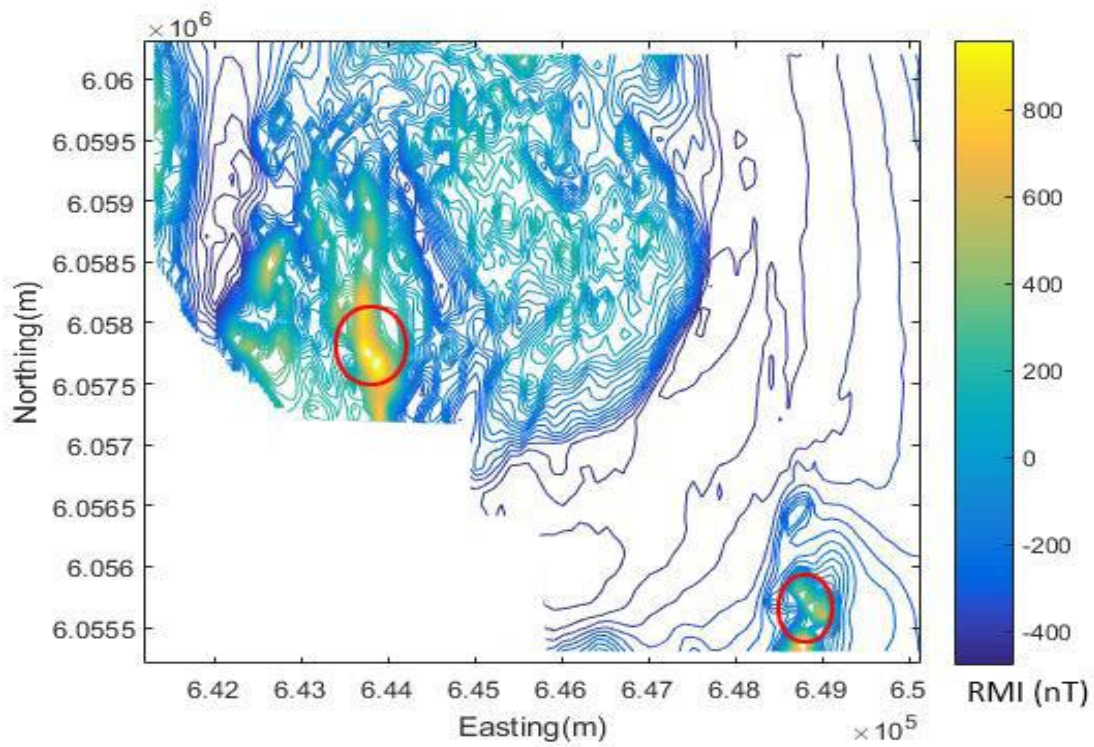


Figure 3.2 Co-location map of EM and MAG anomalies of south Botham Bay block

## 3.2 METHODS

### 3.2.1 Depth estimate from radial frequency spectrum method applied to magnetic data

A magnetic anomaly signal could be considered to be composed of many harmonic waves with different frequencies. And a spectrum refers to the function of the full range of all frequencies of electromagnetic radiation.

If a point source is right at the ground surface, its magnetic signature will be a large amplitude short horizontal scale, like a delta function, so at the source depth the spectrum will be:

$$G_h(\omega_r) = \text{constant} \quad 3.1$$

where  $\omega_r$  is a spatial frequency,  $G_h(\omega_r)$  is the spectrum at depth  $h$ .

If the source is at a depth below surface and we upward continue this, the spectrum will be multiplied by the upward continuation factor:

$$e^{-2\pi(\omega_x^2 + \omega_y^2)^{1/2} h} \quad 3.2$$

where  $\omega_x$  and  $\omega_y$  are spatial frequencies in x and y directions.

Therefore the spectrum at the surface  $G_s(\omega_r)$  will be related to the spectrum at depth  $h$ ,  $G_h(\omega_r)$  by:

$$G_s(\omega_r) = G_h(\omega_r) e^{-2\pi(\omega_x^2 + \omega_y^2)^{1/2} h} \quad 3.3$$

If we take the natural log of both sides of the equal sign:

$$\ln(G_s(\omega_r)) = \ln(G_h(\omega_r)) - 2\pi(\omega_x^2 + \omega_y^2)^{1/2} h \quad 3.4$$

On a semilog graph of radial frequency (on a linear scale) against Fourier amplitude (on a log scale), a straight line should be presented and its slope is inversely proportional to the depth

(Merriam, James. “General Rules for Depth Estimates”. University of Saskatchewan).

A great advantage of radial frequency spectrum method is that it can deal with blocks of data as the HELITEM survey data are of great amount and calculating sampling point by sampling point would be very time-consuming. Therefore the whole survey block is divided into many sub-blocks and each sub-block is used to do the radial frequency spectrum method through a matlab program written by Professor James Merriam.

Hollingdale Lake survey block was divided into 138 sub-blocks and South Botham Bay survey block was divided into 156 sub-blocks as below:



Figure 3.3 Hollingdale Lake sub-blocks division

The radial frequency spectrum method was employed on each sub-blocks of the survey area and two examples of radial frequency spectrum method are demonstrated below (Figure 3.5, Figure 3.6).

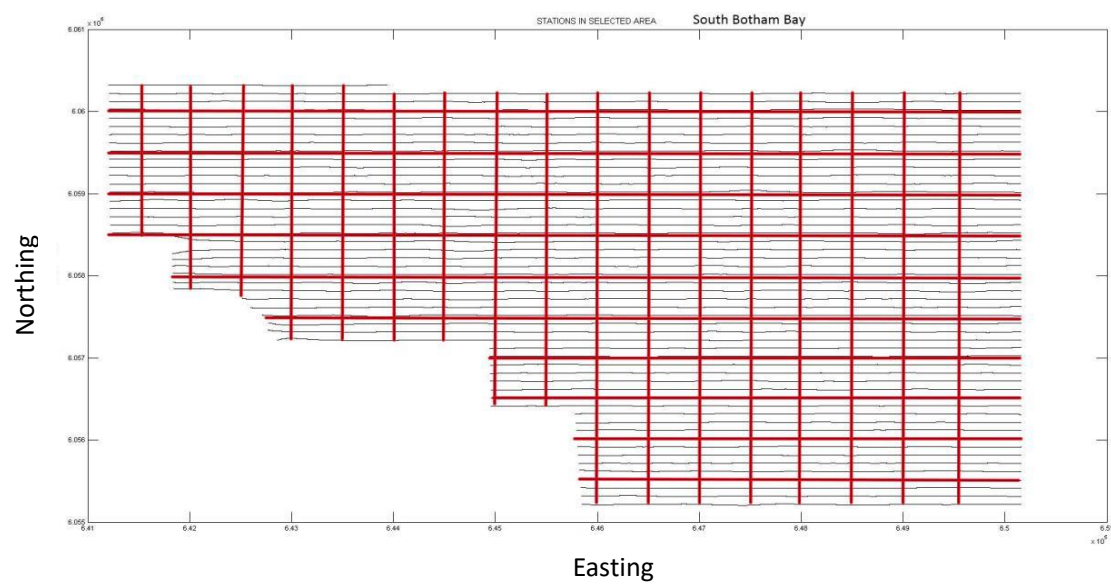


Figure 3.4 South Botham Bay sub-blocks division

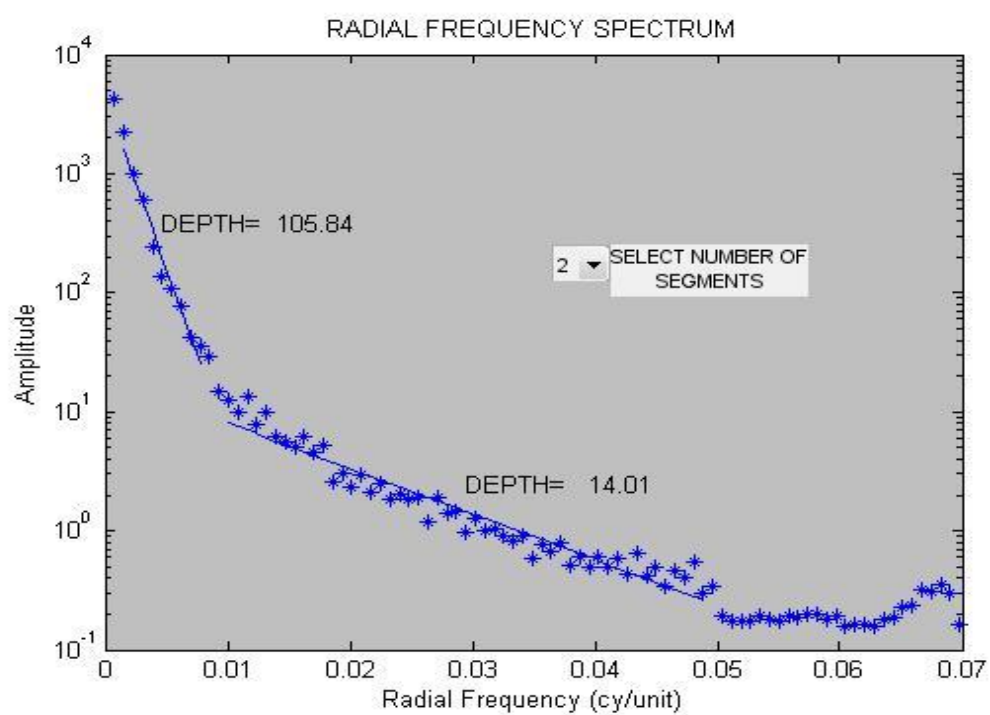


Figure 3.5 Examples of radial frequency spectrum laplace method



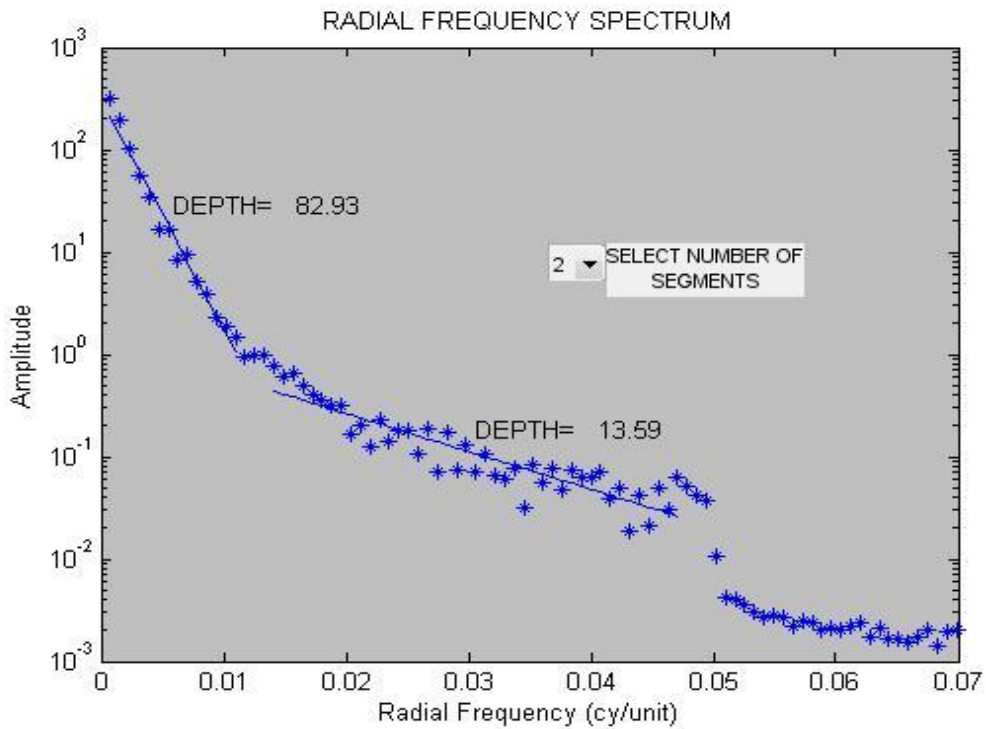


Figure 3.6 Examples of radial frequency spectrum laplace method

The magnetometer was hung on the helicopter platform which was 35 meters above ground. Therefore the depth estimate obtained from above should subtract 35 meters to give the depth of source to surface. For example, the first straight line segment in Figure 3.5 indicates a depth of 82.93m from source to the magnetometer which reveals a depth of 47.93m from source to ground surface. The second segment in Figure 3.5 shows a depth of 13.59m which is smaller than the height of the magnetometer. It is a result of the imperfect zeroing of the filter. The red line segment in Figure 3.6 shows a drop in amplitude and that is caused by gridding flight lines and tie lines.

After applying spectrum method to every sub-blocks in the survey blocks. The results were gridded and contoured into depth estimate maps as shown below:

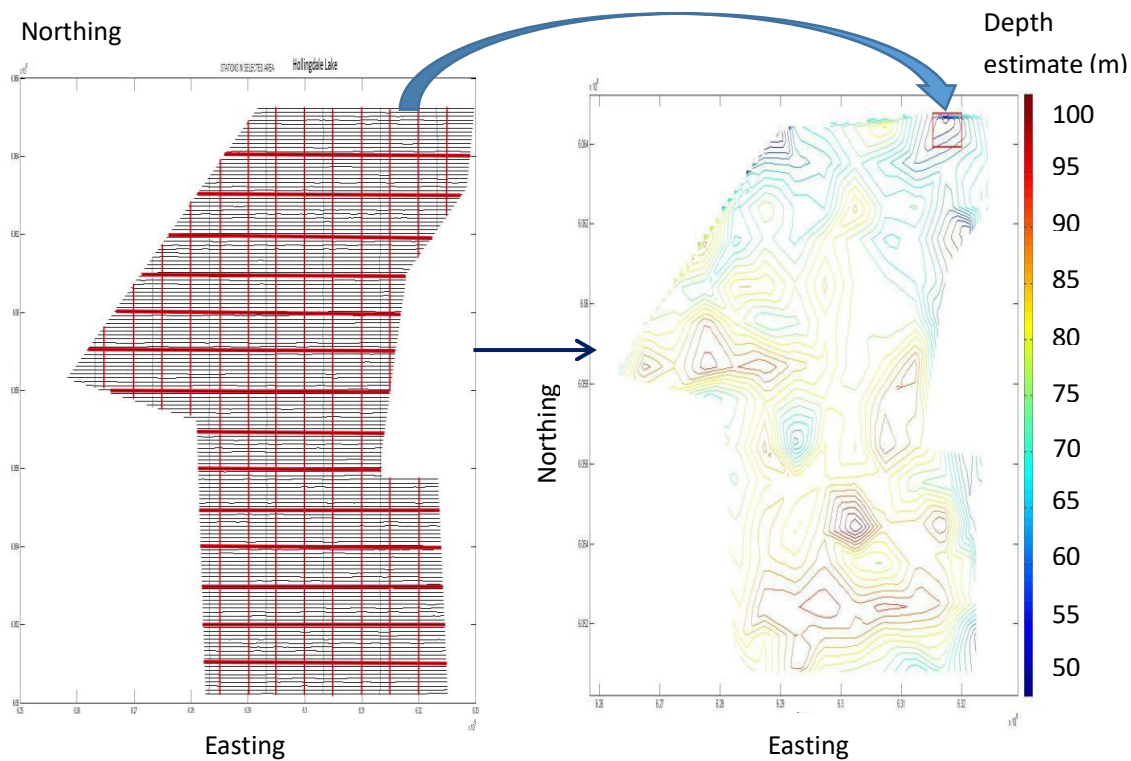


Figure 3.7 Depth estimation of Hollingdale Lake survey block

The contour maps give a direct viewing of where deeper magnetic response exists and where shallower magnetic response is also.

### 3.2.2 Depth estimate from tilt derivative method applied to magnetic data

Tilt derivative (TDR) is a transformed ratio of the horizontal and vertical derivatives (Miller and Singh, 1994) and at a location (x, y) it is given by:

$$TDR(x, y) = \tan^{-1} \left[ \frac{\partial f / \partial z}{\sqrt{(\partial f / \partial x)^2 + (\partial f / \partial y)^2}} \right] \quad 3.5$$

where  $f$  is the total field magnetic anomaly.

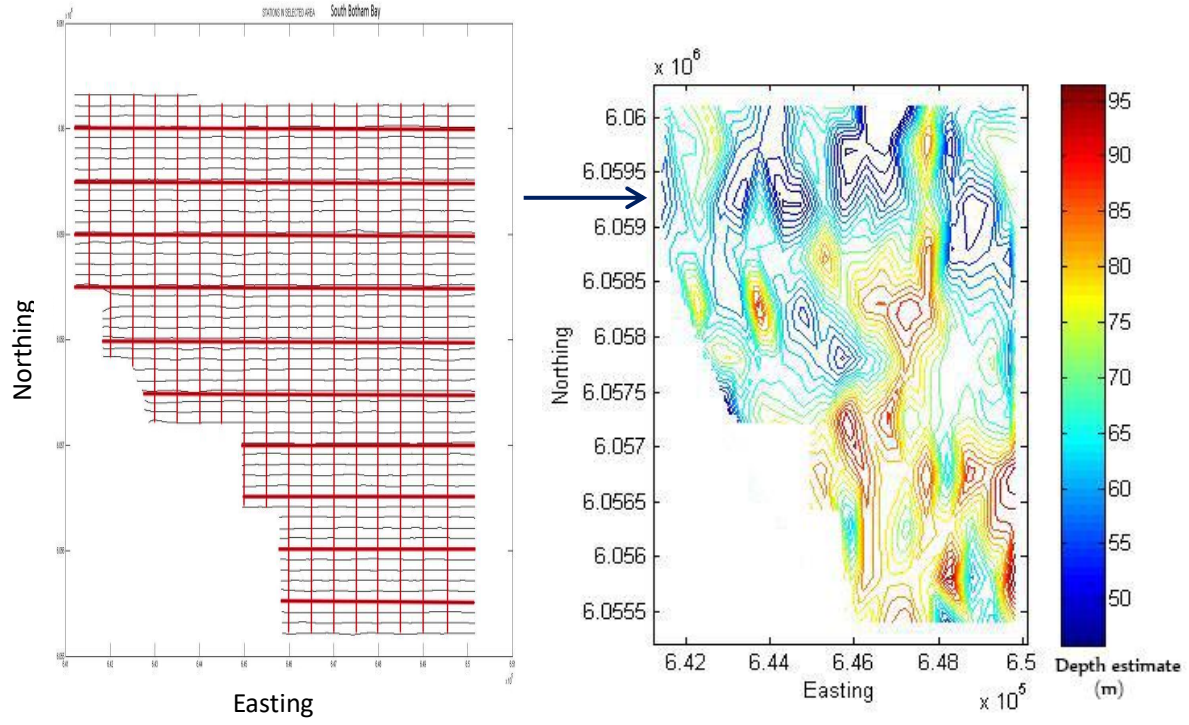


Figure 3.8 Depth estimation of South Botham Bay survey block

It can be treated as an angle (tilt angle) and it is defined as:

$$\theta = \tan^{-1} \left[ \frac{\partial f / \partial z}{\partial f / \partial h} \right] \quad 3.6$$

where

$$\frac{\partial f}{\partial h} = \sqrt{\left( \frac{\partial f}{\partial x} \right)^2 + \left( \frac{\partial f}{\partial y} \right)^2} \quad 3.7$$

$f$  is the total magnetic field and  $\frac{\partial f}{\partial x}$ ,  $\frac{\partial f}{\partial y}$ ,  $\frac{\partial f}{\partial z}$  are the derivatives of the magnetic field in x, y and z directions.

The tilt derivative method assumes a vertical contact model and with that model the tilt angle can be written as (Salem et al., 2007):

$$\theta = \tan^{-1}\left(\frac{H}{z_0}\right) \quad 3.8$$

where  $z_0$  is the depth to the upper boundaries of the source and  $H$  is the horizontal distance from the horizontal location of the contact. Equation 3.6 and 3.8 provide estimates of  $H$  and  $z_0$ .

According to the equation above, if we want to find the contact we need to look at where  $H = 0$  and therefore where the tilt angle is  $0^\circ$ . On the other hand when the tilt angle is  $45^\circ$  and  $-45^\circ$  then  $H = z_0$  and  $H = -z_0$ . The perpendicular distance between the  $45^\circ$  and  $-45^\circ$  contour lines indicates twice the depth of the source.

Tilt derivative method can provide accurate depth estimation and it also can be programmable and applied to block of data which improves the efficiency of the study. Applying this method to the same sub-block as the spectrum method can provide more details of the contact and depth of source at different locations, but it will be much harder to produce a whole block depth estimation contour map. Therefore the tilt derivative method is used after spectrum method to examine targets in detail.

The tilt derivative method is applied to a sub-block in south Botham Bay survey block and  $0^\circ$ ,  $45^\circ$ ,  $-45^\circ$  contour lines are plotted to show the contact as well as the depth to source (Figure 3.9).

At the point that is marked A, the perpendicular distance between  $45^\circ$  and  $-45^\circ$  contour lines is 55.6 meters which indicates the depth from the magnetometer to the top of the source is 27.8m. The height of the magnetometer is 35 meters, so in this example the source is about the ground. Taking into consideration the error, it is suggesting the source is at the surface.

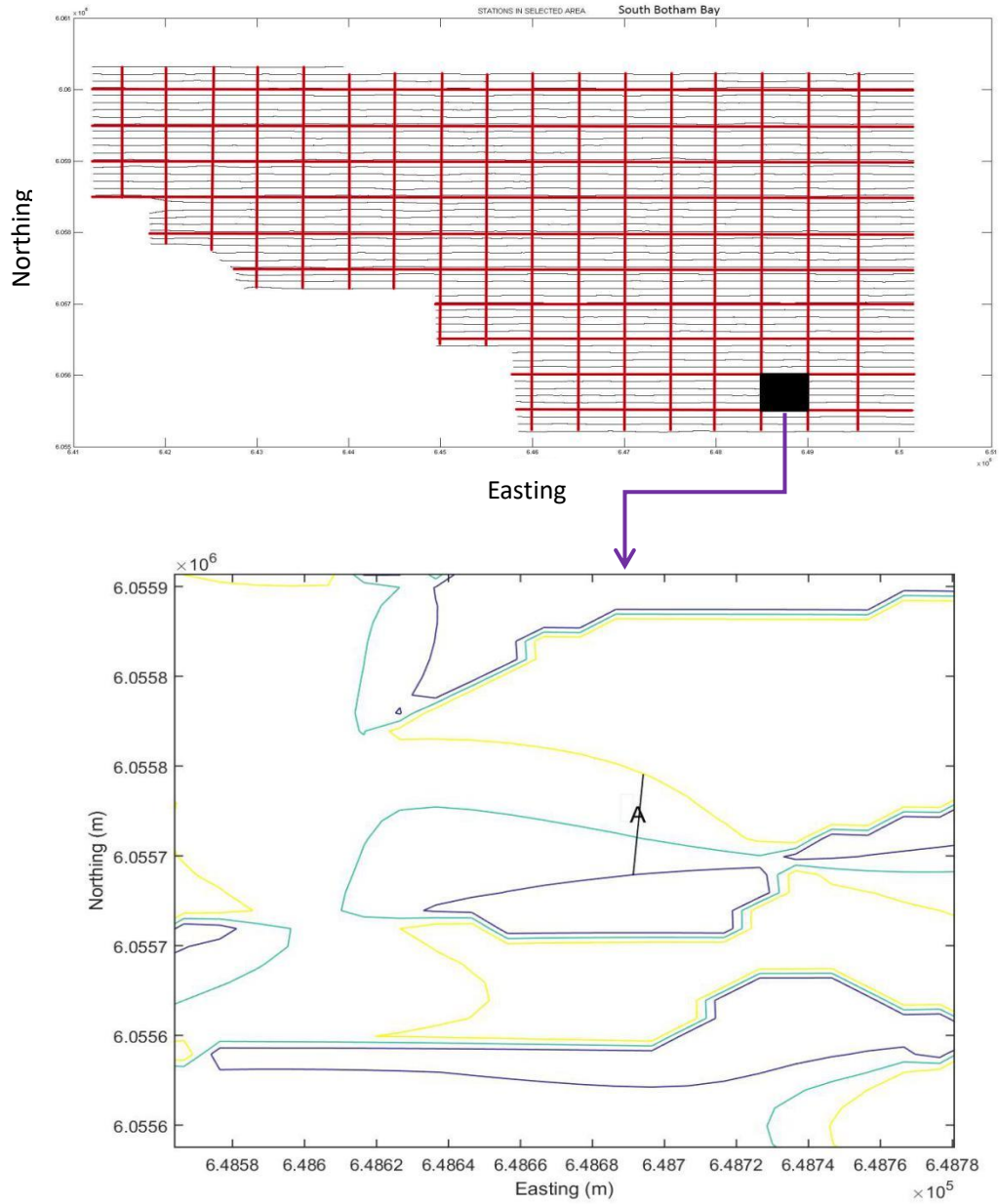


Figure 3.9 Tilt derivative contour map of a sub-block in south Botham Bay survey block. 0° contour line (green line) is plot to show the upper boundaries of the source and 45° (yellow line) and -45° (dark blue line) contour lines are plot to show the depth of contact.

# Chapter 4

## Maxwell Plate Modelling

### 4.1 INTRODUCTION

The last chapter discussed the depth estimate of the potential targets using the magnetic data. This chapter will focus on the depth estimate from electromagnetic data. Electromagnetic plate modelling can also attempt to refine the conductor's depth extent, size, shape and conductivity besides depth.

ElectroMagnetic Imaging Technology (EMIT) developed the geophysical modelling software Maxwell which is widely used in the industry and it is used in this study for thin plate modelling. Maxwell has many advantages such as fast computational speed, relatively easy to learn and it allows users to perturb the starting model by setting initial values for parameters to receive a better fit (Bob, 2014).

Maxwell's thin plate algorithm assumes that the conductive plate is in a very resistive host. Therefore, in order to obtain this approximation, we should use data from the mid-time and late-time channels where the weakly conductive earth response has decayed away (leaving just the conductive response of the target) to do the modelling.

Maxwell can not only do forward modelling, but also inversion modelling. Through forward modelling it is easily noticed that the size, shape, depth and dip angle of one conductor all can affect its electromagnetic response in X and Z components. For example, Figure 4.1 shows how dip angle affects the electromagnetic response in X and Z components. When the conductive

# HELITEM Plate Models

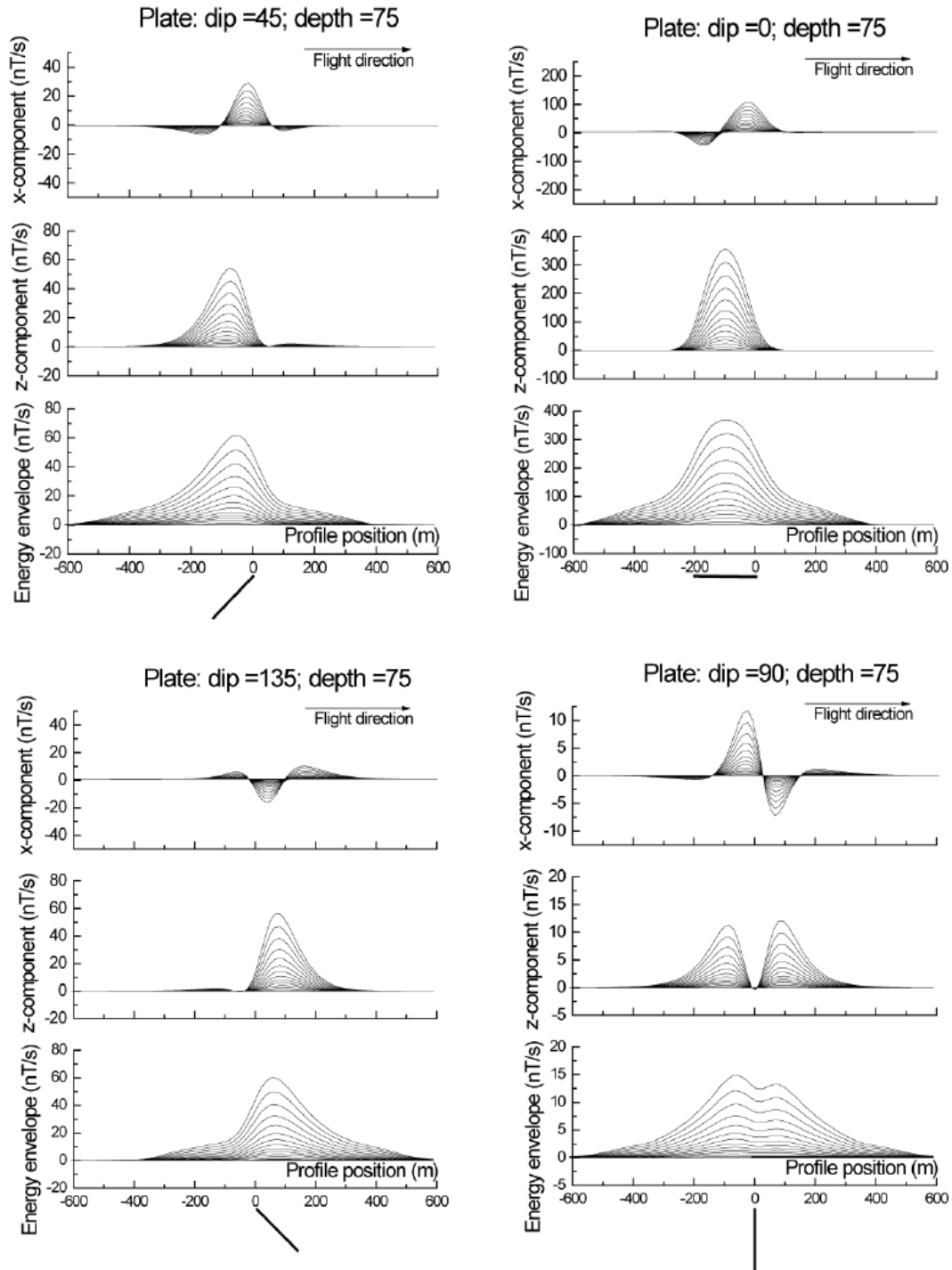


Figure 4.1 Plate modelling with a 200m×200m thin plate and a depth of 75m. Flight direction is from left to right. The black lines on the figure indicate responses from Channel 5 to Channel 30. After Fugro Airborne Surveys (2013)

plate is set horizontal, its Z component electromagnetic response is a single peak right above the target and its X component electromagnetic response is a trough and a peak from west to east. However when the plate is set vertical, its Z component electromagnetic response is a double peak centered on the top of the conductor's location and its X component electromagnetic response is a minor trough - major peak - major trough - minor peak pattern from west to east. When the plate is 45° dipping to the West, its Z component electromagnetic response is a major peak and a minor peak from west to east and its X component electromagnetic response is a trough - peak - trough pattern and an opposite result will be obtained if the plate is dipping to the East.

## **4.2 PROCEDURE**

According to the co-location maps of electromagnetic and magnetic anomalies in chapter 3, two potential areas were selected and found to be good for plate modelling. The first area is in the Hollingdale Lake block which is called Area 1 in this study and the second area is in the South Botham Bay block which is called Area 2.

### **4.2.1 Area 1 thin plate modelling**

Figure 4.2 shows the location of Area 1 where Flight Line L30220 and Tie Line T30971 detected a coincident magnetic and electromagnetic anomaly.

The result of the thin plate modelling of L30220 is shown in Figure 4.3. On the left side, the black line represents the Flight Line L30220 and the red rectangle represents the thin plate conductor that is obtained from the modelling. The top of the conductor is 53.1m. It has a strike length of 133m, a dip extent of 132m, a conductance of 67 Seimens and 40° dipping to the East. On the right side, the black lines are the field data of Z components and X components electromagnetic response along the flight line and the red lines indicate the signals from the modeled plate. Only middle to late channels (channels 15 to 30) are used here. The single plate model has a reasonably good fit of the field data of Flight Line L30220.



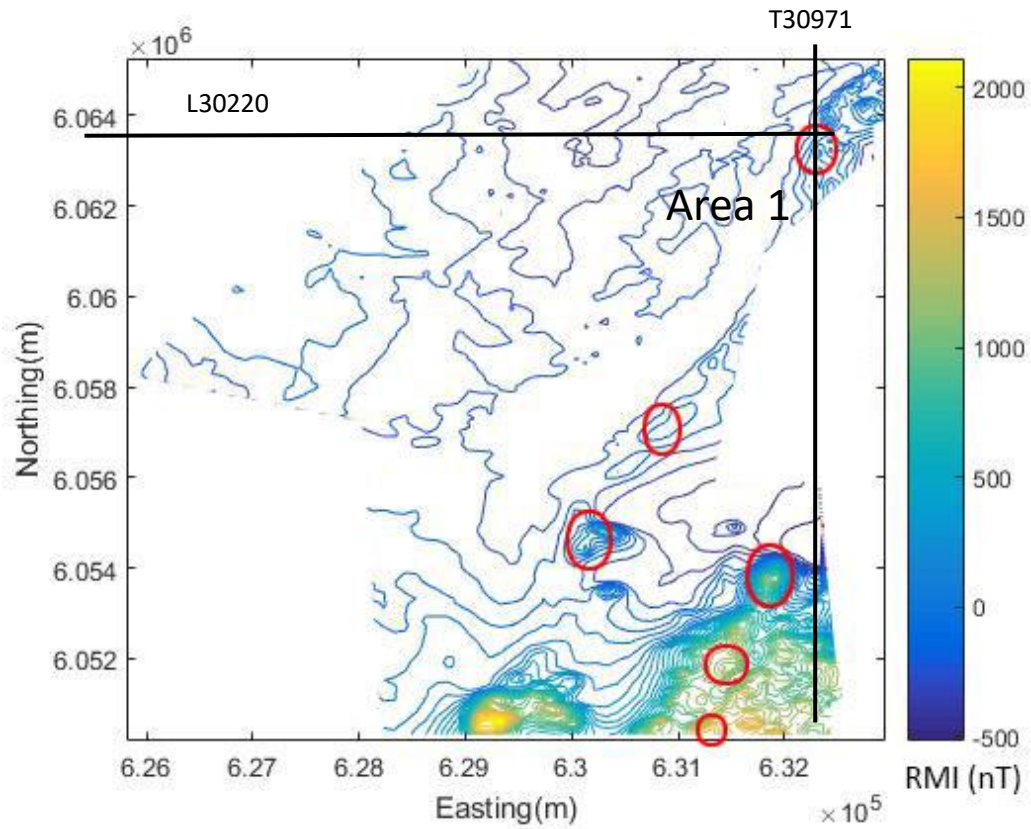


Figure 4.2 Location of Area 1

Then the plate obtained from Flight Line L30220 is used to check against tie line response (Tie Line T30971) as shown in Figure 4.4.

It can be seen that this single plate model also has a good fit with the tie line field data.

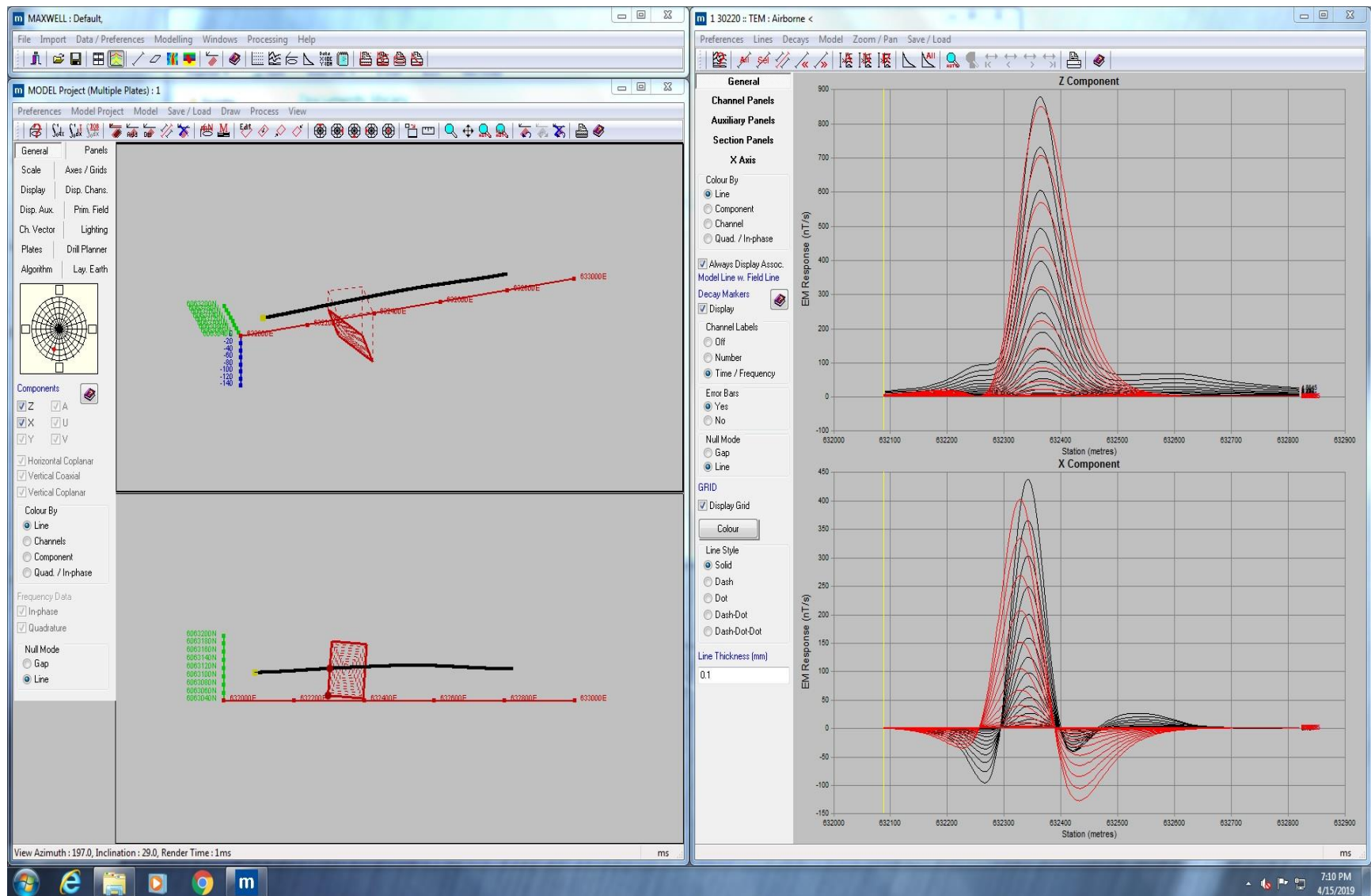


Figure 4.3 Plate modelling of L30220 (Channels 15-30 are shown)

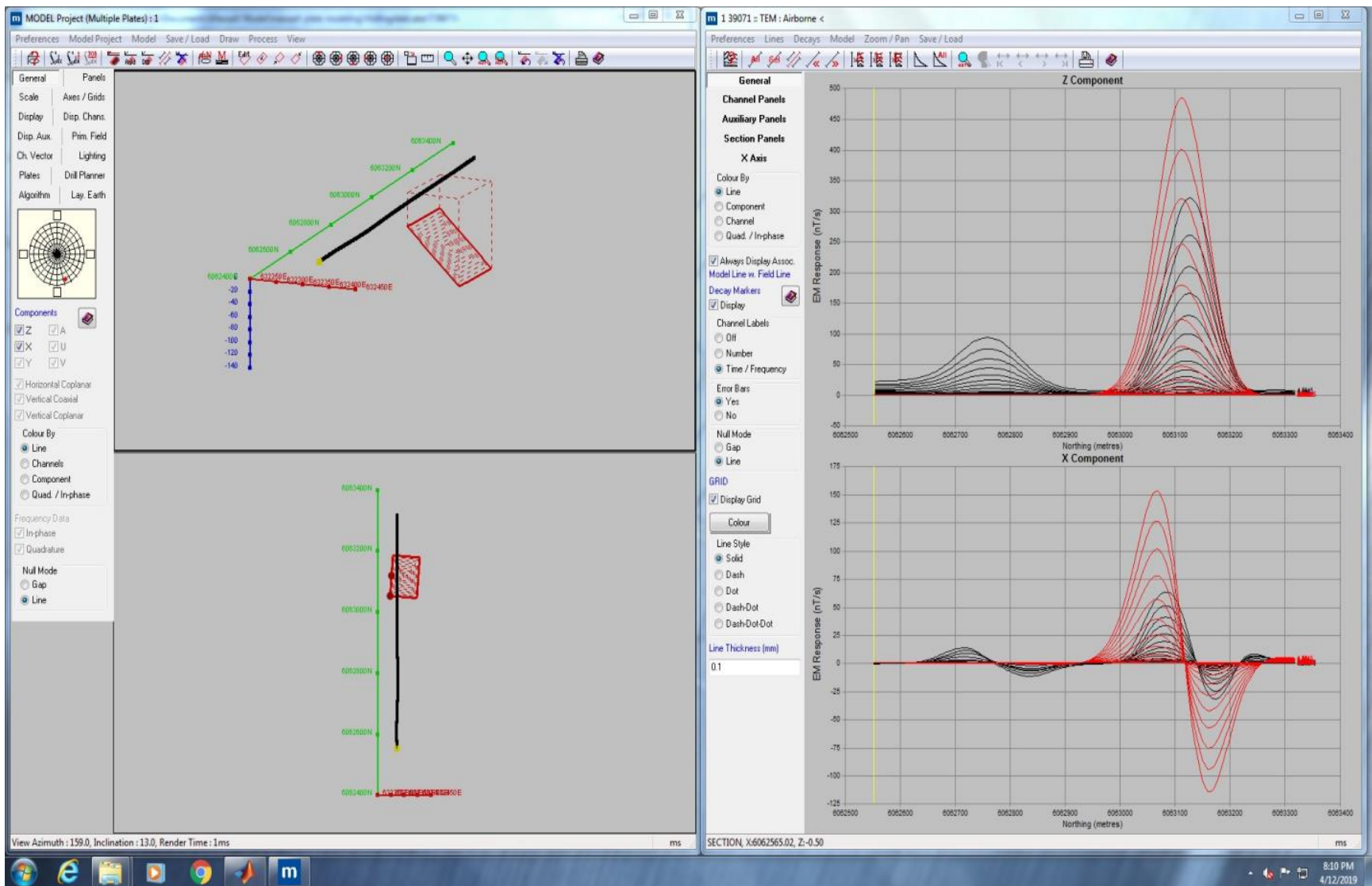


Figure 4.4 Plate modelling of T30971 (Channels 15-30 are shown)

#### 4.2.2 Area 2 thin plate modelling

Figure 4.5 shows the location of Area 2 where Flight Line L12080, L12090, L12100 and Tie Line T19080 detected a coincident magnetic and electromagnetic anomaly.

A combined model using data from Flight Line L12080, L12090 and L12100 is created and two plates are obtained as a result of Maxwell thin plate modelling (Figure 4.6).

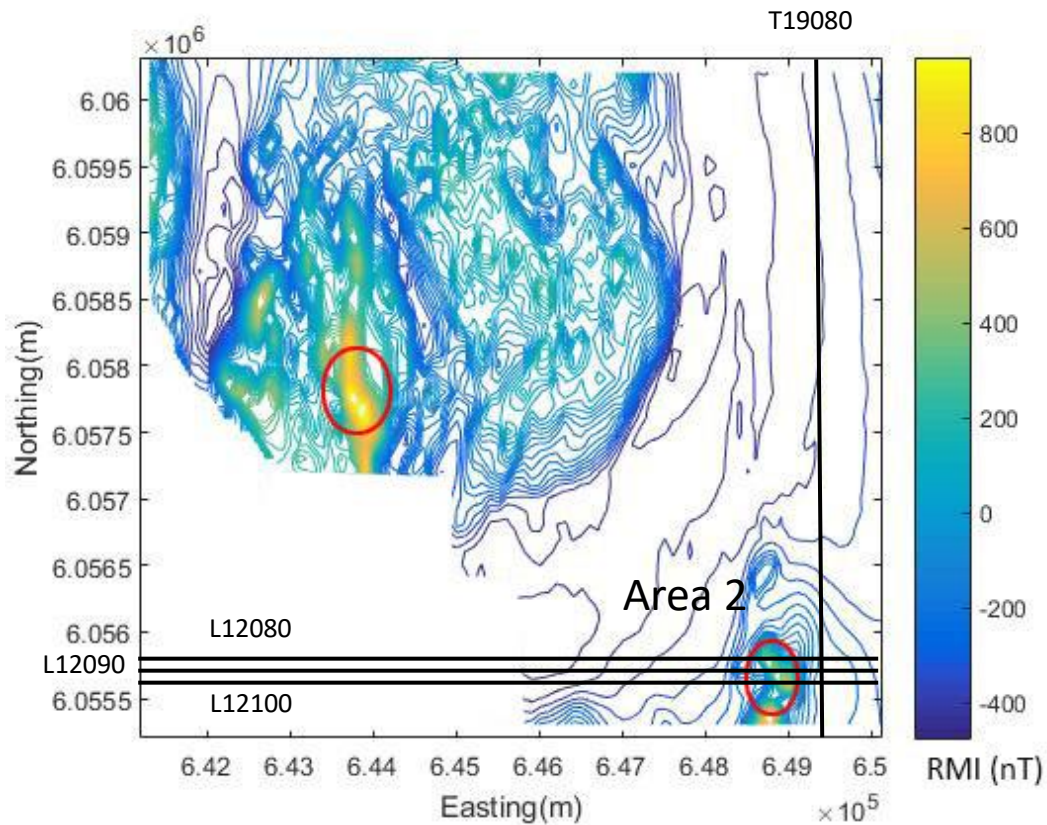


Figure 4.5 Location of Area 2

As shown above in Figure 4.6, the red plate on the west has a depth of 21.6m, a strike length of 290m, a depth extent of 275m, a conductance of 69.5 Seimens and  $65^\circ$  dipping to the West; the blue plate has a depth of 60m, a strike length of 277m, a depth extent of 210m, a conductance of 19.9 Seimens and is almost flat lying. Therefore the red conductor has a steep tilt angle and a shallower depth to surface while the blue conductor is close to horizontal-lying at a larger depth

and also less conductive.

Figure 4.7 shows the Z component and X component electromagnetic response of this two-plate model comparing with the field data along the Flight Line L12080, L12090 and L12100. It can be told that the two-plate model has a reasonably good fit on all three flight lines.

Then the two plates obtained from the combined three flight line model are used to check against tie line response (Tie Line T19080).

As shown in Figure 4.8, this two-plate model has a acceptably good fit with the tie line field data as well.



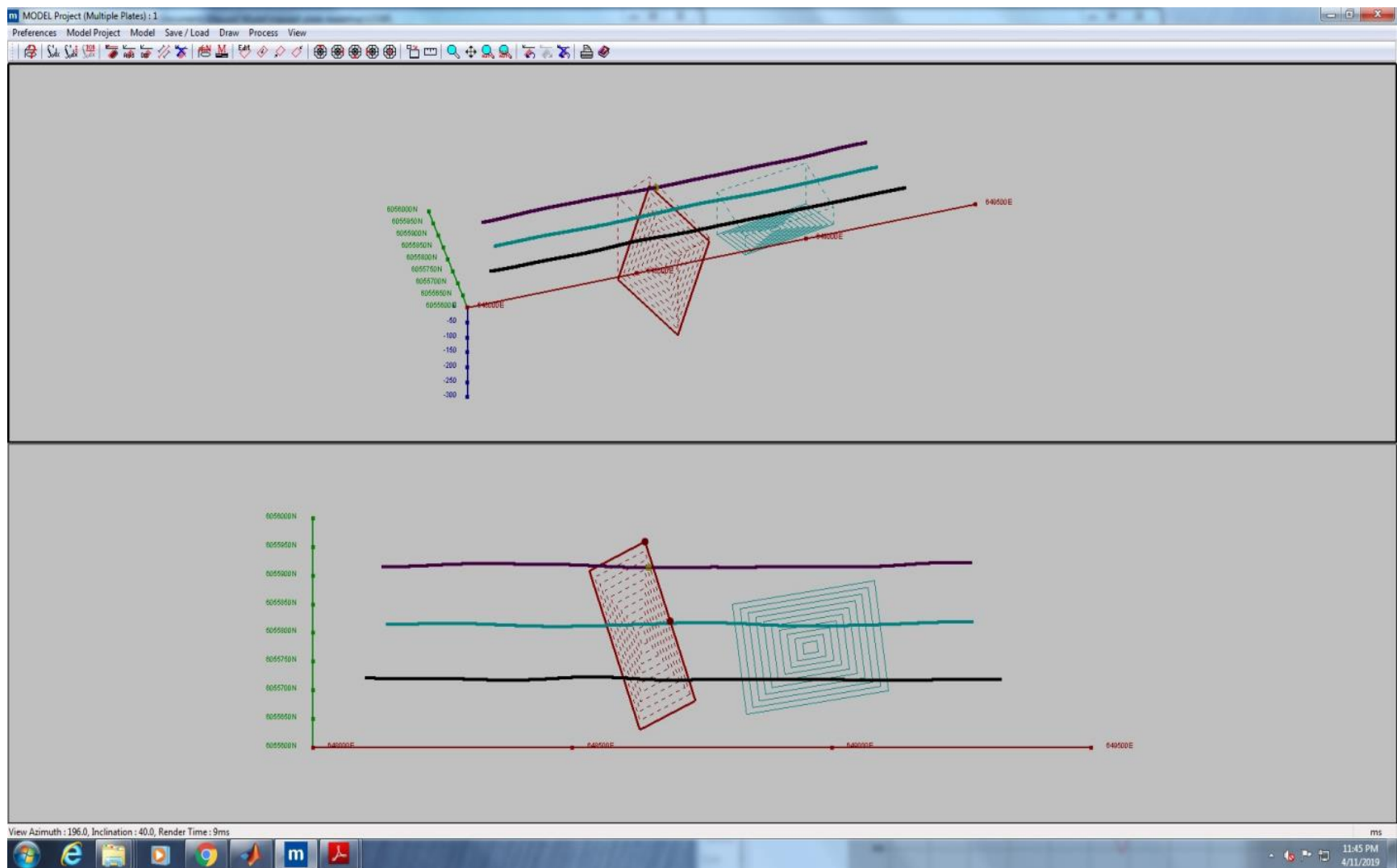


Figure 4.6 Plate modelling of L12080, L12090, L12100

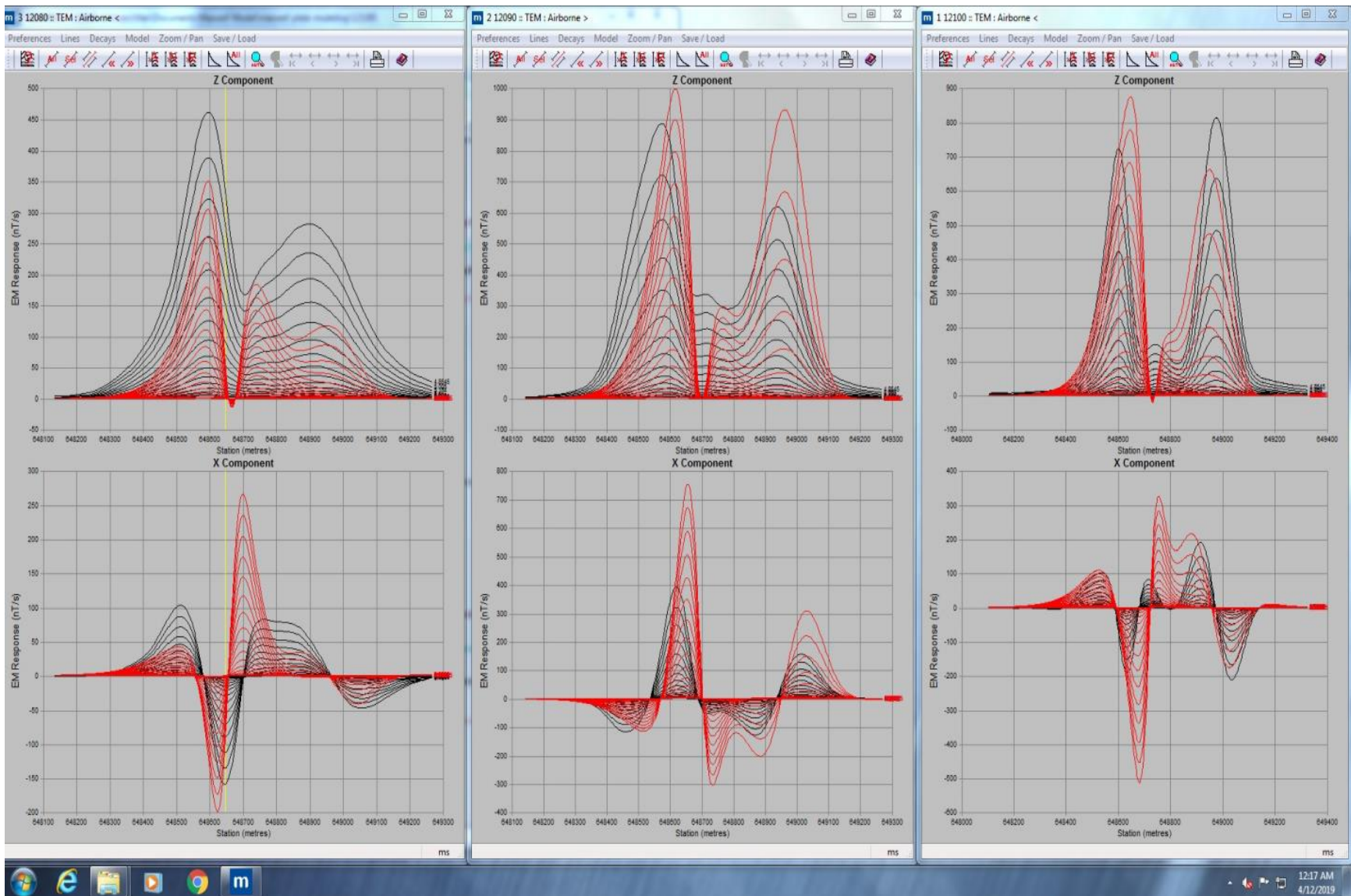


Figure 4.7 Profiles of the two-plate model comparing with field data (Channels 15-30 are shown)

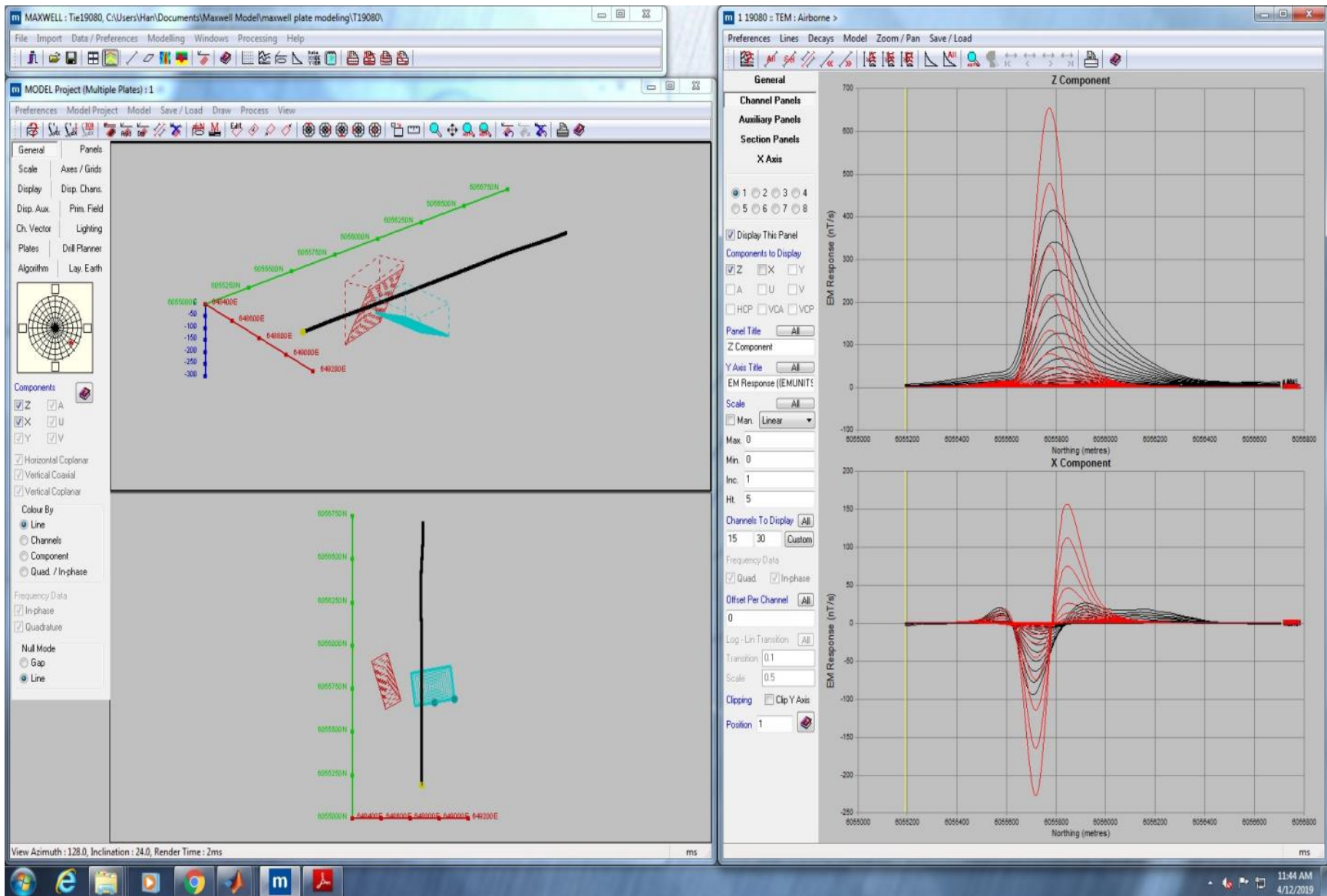


Figure 4.8 Plate modelling of T19080 (Channels 15-30 are shown)



# Chapter 5

## Results

Two potential areas, Area 1 and Area 2, are demonstrated in chapter 4. Both magnetic anomalies and electromagnetic anomalies are detected there and the electromagnetic anomalies are good for the thin plate modelling. Depth estimate of the targets are conducted using magnetic data and electromagnetic data separately in chapter 3 and chapter 4.

Figure 5.1 shows the depth estimate from the Radial Frequency Spectrum method applied to magnetic data in Area 1. The first straight line segment in Figure 5.1 indicates a depth of 71.19m from source to the magnetometer which reveals a depth of 36.19m from source to ground surface (the magnetometer is 35m above ground). Figure 5.2 shows the depth estimate from the Radial Frequency Spectrum method applied to magnetic data in Area 2 and it indicates the depth of the target is 58m from source to the magnetometer and 23m from source to surface.

Figure 5.3 and Figure 5.4 display the results of the depth estimate of tilt derivative method applied to magnetic data in Area 1 and Area 2 separately. The perpendicular distance between  $45^\circ$  and  $-45^\circ$  contour lines indicates twice the depth and in this case Area 1 target has a depth of 58m from source to ground surface and it is suggesting that the Area 2 target is at the surface.

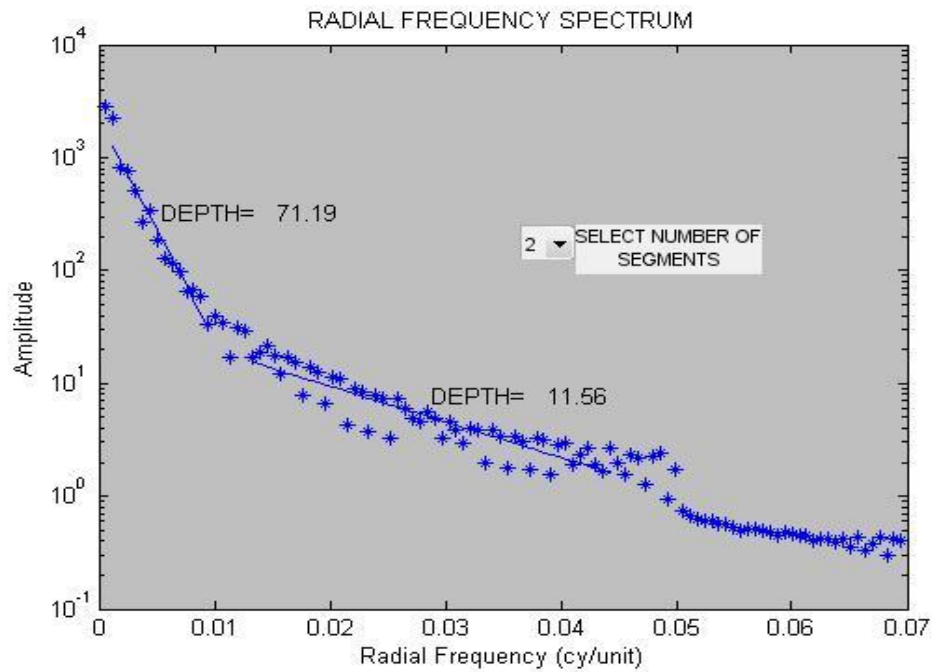


Figure 5.1 Radial frequency spectrum method applied to magnetic data in Area 1

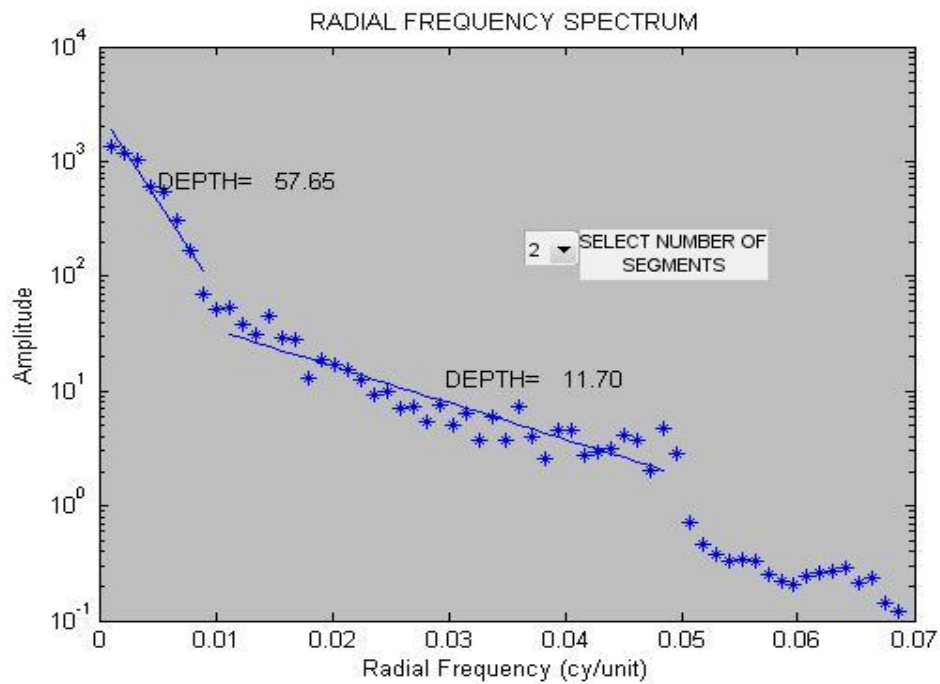


Figure 5.2 Radial frequency spectrum method applied to magnetic data in Area 2

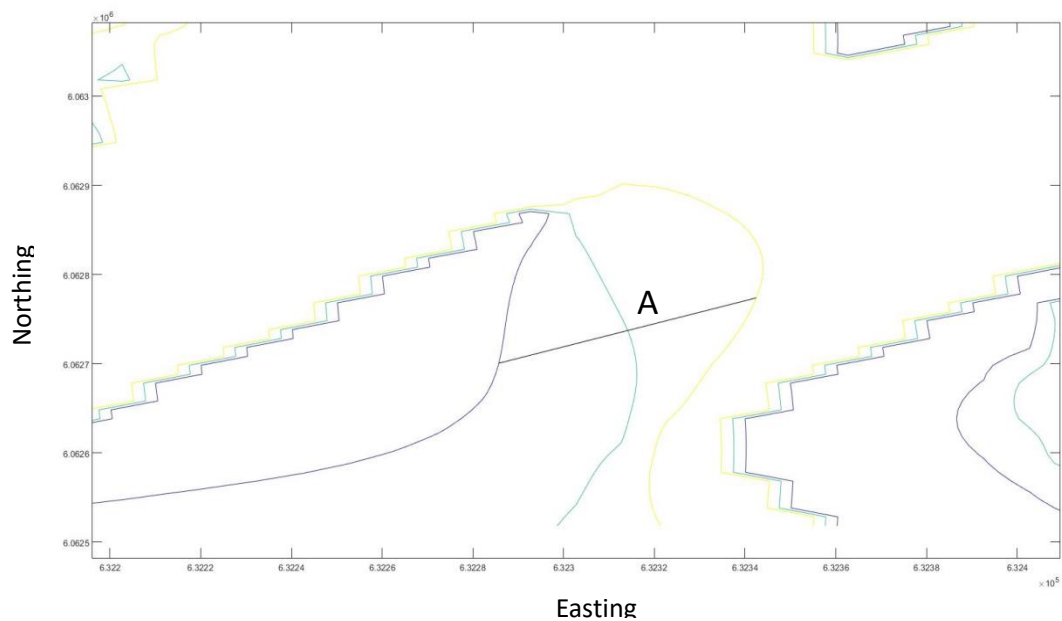


Figure 5.3 Tilt derivative method applied to magnetic data in Area 1

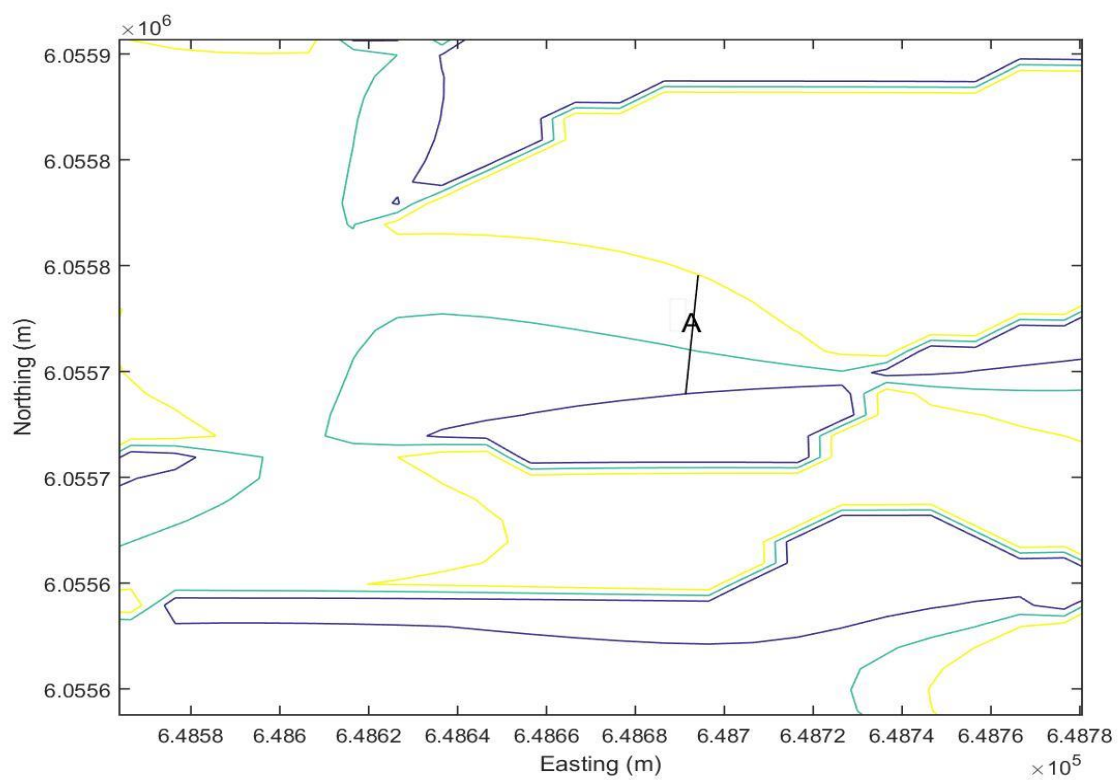


Figure 5.4 Tilt derivative method applied to magnetic data in Area 2

Above results are compared with the Maxwell thin plate models obtained from electromagnetic data in chapter 4 to make sure the magnetic anomalies and the electromagnetic anomalies are reflecting the same source at the same depth (Table 5.1).

	Depth from EM anomaly	Depth from MAG anomaly, radial frequency spectrum method	Depth from MAG anomaly, tilt derivative method
Area 1	53m top of conductor	36m	58m
Area 2	21m top of first conductor, 60m top of second conductor	22m	0m

Table 5.1 Comparison of depth estimate from electromagnetic anomalies and magnetic anomalies

Both depth estimate methods used on the magnetic data have different assumptions and so some differences in depths are expected. From the above table, depths from electromagnetic anomalies are consistent with depths from magnetic anomalies in Area 1 and Area 2. Therefore it is reasonable to say that Area 1 and Area 2 both have sources that are conductive and magnetic. The two areas can be viewed as potential areas for VMS deposits and the Maxwell thin plate models give us the potential targets' orientation and size as well.

# Chapter 6

## Conclusions

In the HELITEM system, the transmitter and receiver coils are attached to a flying helicopter and there is a coil coupling effect produced as a result of the motion of the receiving coil in the static geomagnetic field. The industry assumes that this electromagnetic induction is a constant during a pulse time and corrects it as a part of the leveling. However, in chapter 2 it is proved that the coil coupling effect cannot be viewed as a constant during a pulse time especially in the case of deposits with long time constants and high horizontal magnetic gradients.

Volcanogenic massive sulfide (VMS) deposits which are the potential targets in this study are very likely to be conductive and magnetic at the same time compared to their hosting environment. Figure 3.1 and figure 3.2 are the co-location maps of electromagnetic and magnetic anomalies of Hollingdale Lake block and south Botham Bay block. Contour maps of residual magnetic intensity (RMI) are used as base maps and the red circles indicate where electromagnetic anomalies and magnetic anomalies exist at the same location, but not necessarily at the same depth.

Chapter 3 applied radial frequency spectrum method and tilt derivative method separately to do depth estimate using magnetic data. Chapter 4 used Maxwell thin plate modeling to do depth estimate from electromagnetic data and plate modeling can also refine the conductor's depth extent, size, shape and conductivity. As a result, it is found that the depths from electromagnetic anomalies are consistent with depths from magnetic anomalies in Area 1 (figure 4.2) and Area 2

(figure 4.5). Therefore the two areas both have targets that are conductive and magnetic at the same time and can be viewed as potential areas for VMS deposits.

## **6.1 RECOMMENDATIONS**

This study here investigated on an airborne magnetic and HELITEM survey on Flin Flon area and provided a procedure to locate potential VMS deposits and refine the targets' depth, orientation, depth extent, size, shape and conductivity. However, the thin plate modelling might not perfectly describe the targets in the field. Further ground surveys are needed on the potential areas.

To improve the performance and effectiveness of the HELITEM system, it is necessary to apply a three component magnetometer instead of only measuring the total field of the magnetic data. The coil coupling effect discussed in chapter 2 is not a huge problem. It won't cause a difference at many places, but at places where the magnetic field is highly variable or where electromagnetic time constants are relatively long, by correcting this effect in a better way could provide better estimates of the time constant.

Only two anomalies were fully investigated. Both proved to be co-located in three dimensions as magnetic and conductive targets. Therefore, a full investigation of other anomalies may discover more co-located prospective targets.

## REFERENCES

- Adam, S. (2012). *Detection of Perfect-conducting Targets with Airborne Electromagnetic Systems*. PhD thesis, University of Toronto.
- Bob, L. (2014). Report on Thin Plate Modeling of VTEM data.
- Comparison of different airborne TEM systems. Retrieved July 15, 2017 from [https://geomodel.info/tdem/help/en/airborne\\_tem.htm?id=1](https://geomodel.info/tdem/help/en/airborne_tem.htm?id=1)
- Dawn, Z. (2013). Flin Flon Project 2013 Airborne Magnetic and HELITEM Survey Assessment report.
- Edward, R., Michael, C. (2018). *Electromagnetics*.
- Flin Flon History. Retrieved July 16, 2017 from <https://www.cityofflinflon.ca/history-of-flin-flon>
- Fugro Airborne Surveys, Geophysical Survey Report to BFR Copper & Gold Inc. (2013)
- Galley, A.G., Syme, E.C., & Bailes, A.H. (2007). Metallogeny of the Paleoproterozoic Flin Flon Belt, Manitoba and Saskatchewan. In Goodfellow W.D. (ed.), *Mineral Deposits of Canada: A Synthesis of Major Deposit Types, District Metallogeny, the Evolution of Geological Provinces, and Exploration Methods* (pp. 509-531). Geological Association of Canada.
- Ghosh, M.K. (1972). *Interpretation of Airborne EM (Electromagnetic) Measurements Based on Thin Sheet Models*. PhD thesis. University of Toronto.
- Gibson, H. et al. (2013). Field Trip Guidebook -FT-C3: The Volcanological and Structural Evolution of the Paleoproterozoic Flin Flon Mining District, Manitoba: The Anatomy of a Giant VMS System Open File Report OF 2013-6.

- Grant, F.S. & West, G.F. (1965). *Interpretation Theory in Applied Geophysics*. McGraw-Hill Book Company.
- Hunt, C.P., Moskowitz, B.M., and Banerjee, S.K. (1995). Magnetic properties of rocks and minerals. In Ahrens, T.J. (ed.), *Rock physics and phase relations-A handbook of physical constants* (pp. 189–204). American Geophysical Union.
- Jean, M.L. (2015). Airborne Electromagnetic Systems - State of the Art and Future Directions. *CSEG Recorder*, 40, No.6.
- Jinming, L. (2005). *Goelectric Field and Electrical Exploration* (p.2). Geological Publishing House.
- Keating, P.B. (1988). *The Inversion of Time-domain Airborne Electromagnetic Data Using the Plate Model*. PhD thesis. McGill University.
- Maxwell - Industry Standard Geophysical EM Data Modeling - EMIT. Retrieved from <http://www.electromag.com.au/maxwell.php>
- Merriam, J. (2018). *General Rules for Depth Estimates*. [Unpublished class notes].
- Miller, H.G. and Singh, V. (1994). Potential field tilt - a new concept for the location of potential field sources. *Journal of Applied Geophysics*, 32, 213-217.
- Palacky, G.J. (1987). Resistivity characteristics of geologic targets. In M. Nabighian, editor, *Electromagnetic Methods in Geophysical Applications Volume 1, Theory*, (pp. 53-129). Society of Exploration Geophysicists.
- Reynolds, J. (1997). *An Introduction to Applied and Environmental Geophysics* (pp. 15-89). John Wiley.
- Richard, S. (2010). Airborne electromagnetic methods: applications to minerals, water and hydrocarbon exploration. *CSEG Recorder*, 3, 7-10.



- Robert S. Carmichael (1989). *Practical handbook of physical properties of rocks and minerals*. CRC Press.
- Salem, A., Williams, S., Fairhead, J. D., Ravat, D., and Smith, R. (2007). Tilt-depth method: A simple depth estimation method using first-order magnetic derivatives, *The Leading Edge*, 26, 1502-1505.
- Simard, R-L., MacLachlan, K., Gibson, H.L., DeWolfe, Y.M., Devine, C.A., Kremer, P.D., Lafrance B., Ames, D., Syme, E.C., Bailes, A.H., Bailey, K., Price, D., Pehrsson, S., Lewis, E.M., Lewis, D. and Galley, A.G. (2013). *Geology of Flin Flon area, Manitoba and Saskatchewan (parts of NTS 63K12, 13)* (Geoscientific Report GR2012-2). Manitoba Innovation, Energy and Mines, Manitoba Geological Survey.
- Touloukian, Y. S., Judd, W. R., Roy, R. F. (1989). *Physical Properties of Rocks and Minerals*. Purdue Research Foundation.
- Yusheng, Z., Shuzhen, Y. & Keqin, C. (2011). *Mineral Deposits (3rd Edition)* (pp. 216-222). Geological Publishing House.